Lipid Nanoparticles from *L. meyenii* Walp Mitigate Sepsis through Multimodal Protein Corona Formation

Junsik J. Sung[1], Jacob R. Shaw[2], Josie D. Rezende[1], Shruti Dharmaraj[1], Andrea L. Cottingham[1], Mehari M. Weldemariam[1], Jace W. Jones[1], Maureen A. Kane[1], Ryan M. Pearson[1,2,3*]

1. Department of Pharmaceutical Sciences, University of Maryland School of Pharmacy, 20 N. Pine Street, Baltimore, MD 21201, USA

2. Department of Microbiology and Immunology, University of Maryland School of Medicine, 685 W. Baltimore Street, Baltimore, MD 21201, USA

3. Marlene and Stewart Greenebaum Comprehensive Cancer Center, University of Maryland School of Medicine, 22 S. Greene Street, Baltimore, MD 21201, USA

[*]Address correspondence to:
Ryan M. Pearson, Ph.D.
Associate Professor, Department of Pharmaceutical Sciences
Director, Bio- and Nano-Technology Center
University of Maryland School of Pharmacy
20 N. Pine Street
N525 Pharmacy Hall
Baltimore, MD 21201, US
Phone: 410-706-3257
Email: rpearson@rx.umaryland.edu

Short title: Plant-derived Nanoparticles Mitigate Sepsis

Abstract

Background: Plant-derived nanoparticles (PDNP) are nano-sized particles isolated from various edible plants that contain bioactive components involved in regulating cellular immune responses against pathogenic intrusion and inflammation.

Purpose: This study describes a novel PDNP derived from *Lepidium meyenii* Walp (maca) that efficiently captures pro-inflammatory cytokines and acute phase proteins in its protein corona to enhance survival in two representative lethal models of sepsis.

Methods: Lipid nanoparticles were isolated from maca (MDNP) and triacylglycerols and phytoceramides were identified as major constituents using lipidomics. The physicochemical properties of MDNPs were determined, anti-inflammatory effects of MDNP were evaluated using *in vitro* models and *in vivo* using endotoxemia and cecal ligation and puncture (CLP) polymicrobial sepsis models. Proteomic analysis of MDNP in healthy or LPS-induced inflammatory plasma was used to determine the composition and inflammatory pathways modulated due to the MDNP protein corona.

Results: *In vitro* studies showed that MDNP were non-toxic, reduced macrophage activation, and effectively sequestered pro-inflammatory cytokines to mitigate NF-κB activity under lipopolysaccharide (LPS) stimulation. In a pre-established LPS-induced endotoxemia model, MDNP-treated mice showed significantly reduced systemic pro-inflammatory cytokines and enhanced survival. Untargeted proteomics and pathway analysis of the MDNP protein corona identified an enrichment in acute phase proteins in MDNP-LPS plasma coronas. MDNP treatment also significantly improved survival in the CLP sepsis model in the absence of antibiotics.

Conclusion: This work identified MDNP as an efficient, plant-derived lipid NP that broadly sequesters and neutralizes a compilation of inflammatory mediators in their coronas, offering multimodal therapeutic potential for treating inflammatory diseases.

Key words

Plant-derived lipid nanoparticles, inflammation, cytokines, acute phase response, sepsis, protein corona

Abbreviations

AP-1: activator protein-1, APCS: Serum Amyloid P component, APP: acute phase proteins, APR: acute phase response, AST/SGOT: aspartate aminotransferase, ATL/SGPT: alanine aminotransferase, BMDM: bone marrow derived macrophages, BUN: blood urea nitrogen, Cer(Phyto): phytoceramide , CLP: cecal ligation and puncture, CREA: creatine, DAMP: damage-associated molecular pattern, DAPI: 4',6-diamidino-2-phenylindole, DGDG: digalactosyldiacylglycerol, DLS: dynamic light scattering, DSC: differential scanning calorimetry, FABP4: Fatty Acid Binding Protein 4, FFA: free fatty acids, FITC: fluorescein isothiocyanate, H&E: hematoxylin & eosin, HexCer(phyto): phytohexosylceramide, Hp: haptoglobin, HSP90AA: Heat Shock Protein 90 alpha, IFN-γ: interferon- gamma, IL-1β: interleukin-1beta, IL-6: interleukin-6, IP: intraperitoneal, IV: intravenous, LCN2: lipocalin-2, LPC: lysophosphatidylcholine, LPS: lipopolysaccharide, MDNP: maca-derived lipid nanoparticles, NF-κB: nuclear factor kappa-light-chain-enhancer of activated B cells, NGP4: neutrophilic granule protein, PAMP: pathogen-associated molecular pattern, PC: phosphatidylcholine, PDNP: plant-derived lipid nanoparticle, PEG: poly(ethylene glycol), PI: phosphatidylinositol, PLGA: poly(lactic-co-glycolic acid), Saa1: serum amyloid A1, SEAP: secreted alkaline phosphatase, SerpinA3N: serine protease inhibitor A3N, TG: triglyceride, TLR-4: toll-like receptor-4, TNF-α: tumor necrosis factor-alpha, TP: total protein

Introduction

Edible plant-derived nanoparticles (PDNP) are nanostructured and membrane-enveloped vesicles secreted by plant cells that serve as carriers of various endogenous bioactive substances. Although previously perceived as cellular debris, PDNP are recognized as crucial entities that regulate cell-cell communication and immune responses against pathogens (Shao et al., 2018). The evolving understanding of the biogenesis of PDNP has been described in previous literature (Chafe, 1969; Robarbs and Kidwai, 1969). Briefly, the process initiates with the formation of a trans-Golgi network or early endosome. Plant cells then generate the matured multivesicular endosome that integrate and fuse with the plasmalemma, releasing PDNP through the inward budding of multivesicular endosomes (Li et al., 2018). There are several studies pointing to the potential therapeutic benefits of PDNP, which in some cases demonstrate anti-inflammatory (Yang et al., 2021), antioxidant (Perut et al., 2021), and anti-cancer activity (Wang et al., 2013). This emerging class of naturally derived nanovesicles offers highly advantageous features for use as nanomedicines, exhibiting negligible toxicity or immunogenicity, efficient cellular uptake, and having capacity to deliver a variety of therapeutic agents through re-engineering (Fang et al., 2024).

Cytokine secretions and the acute phase response (APR) are early, systemic immune reactions that develop within minutes to hours as part of the body's early defense mechanism to injury, infection, or immune challenge (Chen et al., 2018; Markanday, 2015a). The APR is triggered by the release of pro-inflammatory cytokines such as interleukin-6 (IL-6), tumor necrosis factor-alpha (TNF-α), interleukin-1b (IL-1β), and others by macrophages, neutrophils, and various immune cells at the site of inflammation (Tanaka et al., 2014). This response triggers the production of acute phase proteins (APP), which are typically undetectable under healthy conditions but increased 10- to 1000-fold during inflammation (Ansar and Ghosh, 2016). These proteins play roles in modulating inflammation, enhancing pathogen clearance, and promoting tissue repair (Ehlting et al., 2021). The APR is generally recognized as beneficial for restoring homeostasis disturbed by such injuries, however, APP have been described to elicit a range of functions to induce pro- or anti-inflammatory responses. During severe inflammatory responses like sepsis, a dysregulated APR can potentiate the inflammatory response leading to coagulopathy, organ failure, and even death (Castellheim et al., 2009; Markanday, 2015b; Zhang and Ning, 2021).

Several groups have developed strategies to mitigate the inflammatory response by sequestering pro-inflammatory cytokines (Lasola et al., 2020). Multiple studies highlight that the use of membrane-coated nanoparticles that mimic biological cell membranes to trap and neutralize these inflammatory cytokines (Khatoon et al., 2022). By acting as macrophage decoys, these nanoparticles can be developed to bind and neutralize endotoxins, pro-inflammatory cytokines, and even venoms that would contribute to negatively contribute to survival outcomes (Thamphiwatana et al., 2017).

147 Similarly, neutrophil membrane-coated nanoparticles are produced using neutrophils
148 isolated from mouse bone marrow after LPS stimulation (Zhang et al., 2024). The
149 process involves membrane extraction, incubation, and extrusion or sonication with
150 polymeric NP cores. These membrane-camouflaged nanoparticles reduce inflammation
151 by binding and neutralizing endotoxins and cytokines such as IL-6, and TNF-α (Shen et
152 al., 2019; Thamphiwatana et al., 2017). A study showed that IL-6 can be effectively
153 captured and neutralized using chitosan/hyaluronic acid polymeric nanoparticle that
154 have antibodies immobilized on the surface (Lima et al., 2018). Moreover,
155 telodendrimers were developed to bind LPS and pro-inflammatory cytokines through
156 controlling hydrophobic and charge-based interactions (Shi et al., 2020a), and
157 poly(ethylene glycol) (PEG) hydrogels were developed to capture and neutralize
158 histones to improve sepsis survival (Koide et al., 2021a). Despite these advancements,
159 the complex synthesis and formulation required for these designs to sequester pro-
160 inflammatory mediators presents a significant challenge to clinical translation. As a
161 result, there is critical need to develop simpler anti-inflammatory strategies that can
162 sequester multiple inflammatory mediators to mitigate pro-inflammatory responses to
163 augment sepsis survival.
164 *Lepidium meyenii* Walp*,* also referred to as maca, is a biennial root plant
165 indigenous to the Peruvian Andes. Maca possesses high contents of fiber, amino acids,
166 fatty acids, and other essential nutrients, while also containing various bioactive
167 compounds that are involved in integral cellular activities within plants (Wang and Zhu,
168 2019). Several studies have shown that maca alleviates fatigue (Zhu et al., 2022),
169 oxidative stress (Fei et al., 2022), tumor formation (Cao et al., 2023), and inflammation
170 (Yang et al., 2023). However, studies have focused on the raw material or crude extract,
171 which contains mixture of different active ingredients, to evaluate in disease models (Fei
172 et al., 2020; Tenci et al., 2017). Despite these known advantages, maca remains
173 relatively underexplored.
174 This investigation demonstrates the isolation, characterization, and therapeutic
175 development of a PDNP isolated from maca root, termed maca-derived lipid
176 nanoparticle (MDNP), for the treatment of severe inflammation as exemplified using *in*
177 *vitro* and *in vivo* models of lipopolysaccharide (LPS)-induced endotoxemia and
178 polymicrobial sepsis. MDNP were isolated and characterized for physicochemical
179 properties, as well as lipid composition using lipidomic analysis. The toxicity profile of
180 MDNP was then established prior to determining their uptake profile and anti-
181 inflammatory properties. *In vitro*, MDNP efficiently sequestered multiple pro-
182 inflammatory cytokines, which led to comprehensive *in vivo* assessment of their
183 biodistribution and therapeutic activity. Therapeutic administration of MDNP to LPS-
184 challenged mice led to significant reductions in plasma pro-inflammatory cytokines,
185 reductions in inflammation-induced organ damage, and improved survival. When
186 nanoparticles are introduced into a biological fluid, they are rapidly covered by a layer of

biomolecules known as the biomolecule corona (or protein corona) (Pearson et al., 2014; Shaw and Pearson, 2022). To identify the mechanism by which MDNP elicited its anti-inflammatory effects, we performed untargeted proteomics analysis of the MDNP protein corona to uncover the inflammatory mediators sequestered by MDNP and corresponding pathways and upstream regulators modulated. MDNP was found to sequester and neutralize a variety of APP, which promote the propagation of pro-inflammatory immune responses, in addition to pro-inflammatory cytokines. Lastly, the efficacy of MDNP was assessed using a clinically relevant mouse model of polymicrobial sepsis and found to significantly increase survival. These results demonstrate the potential of MDNP as an abundant, cost effective, naturally derived therapeutic agent for use as a multimodal intervention for a variety of inflammatory diseases due to their ability to sequester a broad spectrum of inflammatory mediators.

Results

Isolation and characterization of maca-derived lipid nanoparticles (MDNP)

PDNPs were isolated from maca juice using differential ultracentrifugation and density gradient sucrose gradient centrifugation **(Figure 1**) (Sung et al., 2019). MDNP accumulated at the interface of 20/35% sucrose gradient, and the recovery was approximately 4 mg per 30 g of maca powder (**Figure 1B,C**). TEM revealed that MDNP displays a spherical morphology, and their core structure was consistent with that of solid lipid nanoparticles (**Figure 1D**). Size and zeta potential of MDNP measured an average of 174.5 nm and -9.6 mV, respectively **(Figure 1E)**. We next assessed the stability of MDNP at multiple temperatures. MDNP could tolerate a freeze and thaw cycle and were stable at 4°C for up to 6 days, the maximum length of time tested. All different temperature storage conditions kept MDNP stable except for room temperature (RT), where after 3 days the size was significantly increased (**Figure 1F**). The sizes and zeta potential of MDNP were also stable upon lyophilization (**Supplementary Figure S1**). Differential scanning calorimetry (DSC) analysis determined the summit of melting peak of MDNP, which was measured as 74.3°C (**Figure 1G**).

To determine the lipid composition of MDNP, untargeted high throughput lipidomics was performed. A bar graph (**Figure 1H**) and a pie/vertical slice chart (**Figure 1I**) shows the total lipid abundance and ratio in percentage of each component in MDNP. The lipidomics identified a total of eight individual lipids in four categories including sphingolipids, galactolipids, neutral lipids, and phospholipids (**Supplementary Figure S2**). The most prevalent species within the MDNP was the triglyceride (TG) subclass with 51 identifications (77.45%), followed by phytoceramide (Cer (Phyto); 14.77%), phytohexosylceramide (HexCer (Phyto)) (2.7%), free fatty acids (FFAs) (1.95%), digalactosyldiacylglycerol (DGDG) (0.72%), phosphatidylcholine (PC) (0.96%), phosphatidylinositol (PI) (0.85%), and lysophosphatidylcholine (LPC) (0.13%).

The complete protein compositional analysis of MDNP using UPLC-MS/MS revealed undetectable levels of proteins that could be linked to plant databases from Uniprot and the Plant Proteome Database. This aligns with our lipidomics results indicating that MDNP is primarily composed of lipids, with minimal or no associated protein content. Overall, these data demonstrate the successful isolation, purification, and characterization of MDNP from bulk maca extract.

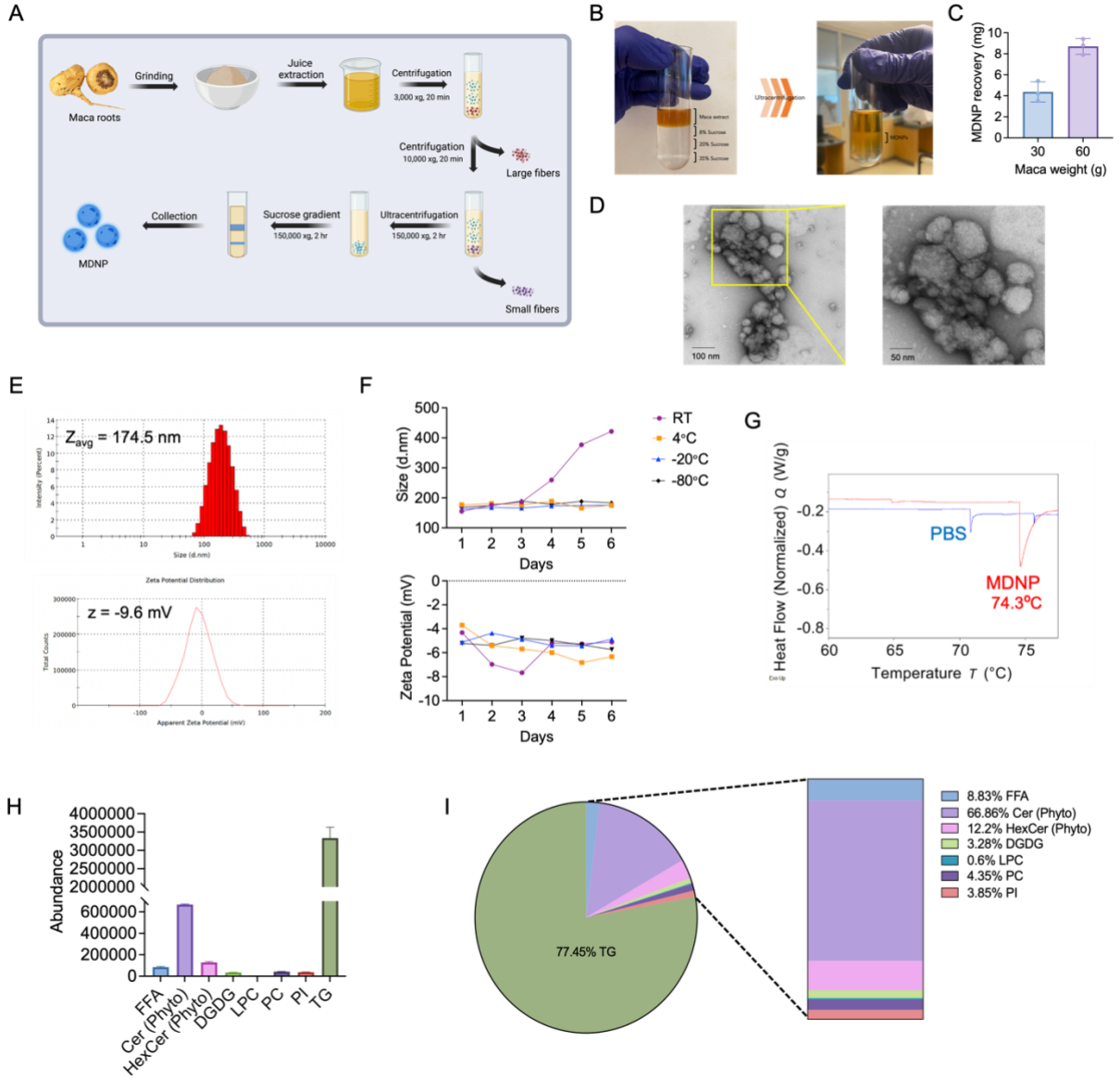

Figure 1. Isolation and characterization of MDNP. (A) Schematic representation of the isolation process for maca-derived lipid nanoparticles (MDNP). (B) Before and after images of MDNP isolation. MDNP were isolated and purified from maca extract by sucrose density gradient purification. (C) MDNP recovery from pure maca powder. (D) A representative TEM image of MDNP. (E) Room temperature measurement of size (174.5 nm) and zeta potential (-9.6 mV) of freshly isolated MDNP. (F) Storage stability test of MDNP under various storage conditions up to day 6. (G) Heat flow curve of MDNP measured by differential scanning calorimetry showing the summit of melting peak at 74.3 ºC. (H) Lipid extraction and component analysis by liquid chromatography coupled to high resolution LC-MS/MS revealed eight different lipids (TG, Cer, HexCer, DGDG, LPC, PC, PI and FFA). Bar graph shows abundance of lipids. (I) Pie graph shows the whole ratio of each component and the vertical slice magnifies the smaller portion of composition excluding TG. N=3/group.

232 ***In vitro* cytotoxicity, internalization, and therapeutic effect of MDNP**
233 To analyze potential toxicity, BMDM were treated with MDNP (1 mg/mL) for 8
234 hours prior to flow cytometry analysis to measure viability and apoptosis (**Figure 2A**).
235 MDNP treatment did not affect the cell viability or induce apoptosis. Furthermore, we
236 observed a time-dependent cellular uptake of Cy5.5-labeled MDNP using BMDM
237 (**Figure 2B**). The quantitative measure of mean fluorescence intensity (MFI) from the
238 confocal microscopy images can be found in **Supplementary Figure S3**. These
239 findings demonstrate the MDNP are non-toxic and efficiently internalized by BMDM.
240 BMDM were treated with LPS followed by MDNP to assess their ability to
241 mitigate immune activation. The observed decrease in CD80 (reduced but not
242 significant), CD86, and MHCII expression following MDNP treatment suggests that
243 MDNP reduced macrophage activation, contributing to a decreased pro-inflammatory
244 response (**Figure 2C-E**). Modulation of macrophage polarization is one of the strategies
245 to modulate inflammation, support tissue regeneration and reestablish disrupted
246 homeostasis(Parisi et al., 2018). We also measured a reduction in CD206 as a marker
247 of anti-inflammatory M2-like macrophages, suggesting MDNP induced a shift in
248 macrophage phenotype towards a more undifferentiated or M0-like state (**Figure 2F**).
249 These results indicate that MDNP can impact the activation status of macrophages
250 suggesting that they aid in shifting their profile towards a more balanced and neutral
251 immune response.
252 To assess the anti-inflammatory effects of MDNP, we investigated its prophylactic
253 and therapeutic activity by treating MDNP on LPS-challenged BMDM. In the
254 prophylactic setting, MDNP was treated for 8 hr prior to 4 hr LPS exposure (**Figure 2G**).
255 However, it did not significantly attenuate the release of pro-inflammatory cytokines (IL-
256 6 and TNF-α) (**Figure 2H,I)**. In the therapeutic setting, BMDM were challenged with
257 LPS for 4 hrs prior to the treatment of MDNP for 8 hr (**Figure 2J**). The result shows that
258 pro-inflammatory cytokines including IL-6, and TNF-α induced by LPS were significantly
259 reduced, whereas IL-1β, and IFN-γ were only slightly reduced (**Supplementary Figure**
260 **S4**). Furthermore, additional testing was conducted on the crude extract after MDNP
261 isolation to determine if it possesses any anti-inflammatory efficacy; however, no
262 cytokine reduction was detected (**Supplementary Figure S5**). These results suggested
263 that MDNP can reduce pro-inflammatory responses, and the anti-inflammatory
264 component of maca is the purified MDNP.
265

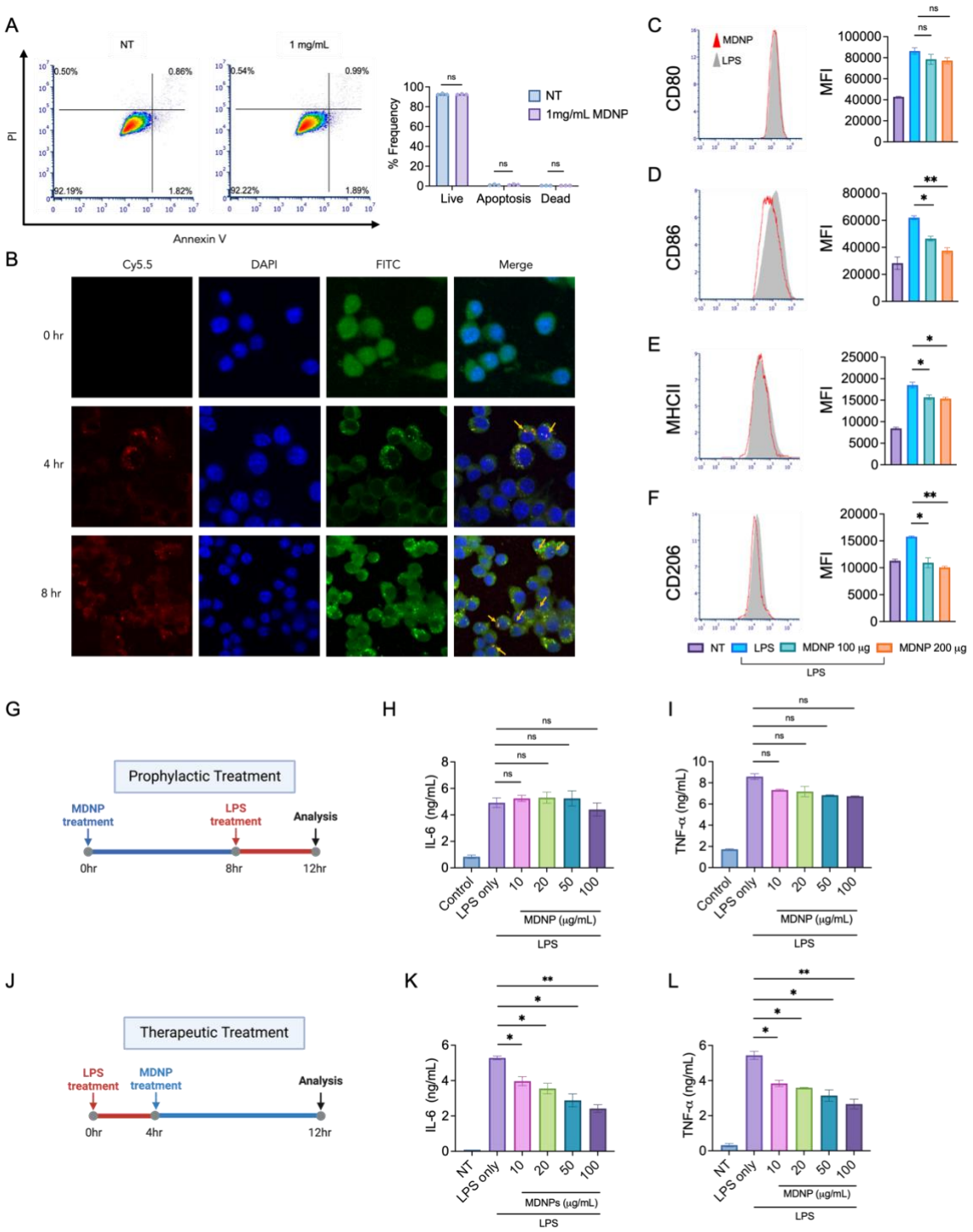

Figure 2. *In vitro* cytotoxicity, cellular internalization, immunomodulation and therapeutic effects against LPS-induced inflammation. (A) PI/Annexin V assay by flow cytometry displayed that treatment with higher concentration (1 mg/mL) of MDNP did not induce any significant toxicity in BMDM. Quantitative analysis of live, apoptotic, and dead cells after MDNP treatment is accompanied. (B) Cy5.5 labeled MDNP were gradually internalized by BMDM after 4 and 8 hrs. Cells were stained with DAPI and FITC-PI to visualize the nucleus and F-actin, respectively. (C-F) Immunomodulatory activity of MDNP in LPS inflamed BMDM showed reduction in M1 (CD80, CD86, MHCII) and M2 (CD206) markers. (G) A timeline for prophylactic treatment. Prophylactic approach did not make significant change in levels of (H) IL-6 and (I) TNF-α. (J) A timeline for therapeutic treatment. Therapeutic treatment displayed significant reduction of (K) IL-6 and (L) TNF-α. Data are expressed as mean ± SD (n=5). Data are expressed as mean ± SD (n=3). *P<0.05, **p<0.05 versus LPS control group.

Sequestration of cytokines and mitigation of NF-κB activation

Interleukin-6 (IL-6) and tumor necrosis factor-α (TNF-α) are well known to be involved in pathogenesis of chronic inflammation, autoimmune diseases, and cancer (Hirano, 2021; Popa et al., 2007). Utilizing data from the *in vitro* anti-inflammatory assay, an investigation was conducted to confirm whether MDNP possess the capability to sequester pro-inflammatory cytokines in the absence of cells. In a time-dependent experiment, BMDM were treated with 100 ng/mL LPS for 4 hrs, then the supernatant rich in inflammatory cytokines was incubated with 100 μg/mL MDNP for up to 24 hrs (**Figure 3A**). ELISA analysis of these supernatants indicated a gradual decrease in IL-6 levels, with a maximum of 48% reduction after 8 hrs (**Figure 3B**). A similar trend was observed for TNF-α levels, with a 28% reduction over the same time period (**Figure 3C**). Optimization of MDNP concentration revealed concentration-dependent cytokine sequestration properties of MDNP and 100 μg/mL MDNP exhibited the most significant sequestration of IL-6 and TNF-α, whereas PLGA nanoparticle (as control) did not display any cytokine sequestration properties (**Supplementary Figure S6**). We also confirmed the ability of MDNP to sequester recombinant IL-6 to exclude the possibility

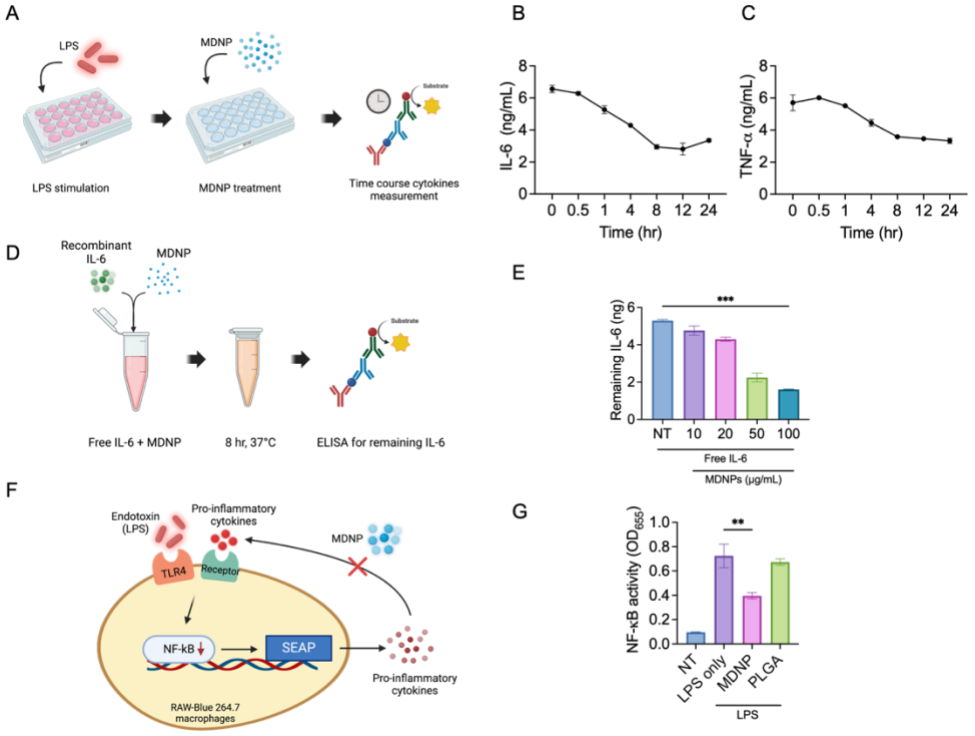

Figure 3. *In vitro* sequestration of pro-inflammatory cytokines from LPS-induced bone marrow derived macrophages. (A) Time course reduction of LPS-stimulated pro-inflammatory cytokine by treatment of MDNP. 8 hr time point exhibited the most significant reduction for both (B) IL-6 and (C) TNF-α. (D) Recombinant IL-6 was sequestered through incubation with MDNP ex vivo without cellular interaction. (E) 100 μg/mL MDNP was the most effective concentration to remove IL-6 protein. (F) Expression of NF-κB in in RAW-Blue 264.7 cell is suppressed by the treatment of MDNP. (G) NF-κB activity level is downregulated after treatment of MDNP. PLGA was used as a control to show different effect on NF-κB. All data are expressed as means ± SD (n=5). **p<0.05, ***p<0.005, and ****p<0.0005 versus LPS or NT control group.

283 of other proteins contributing to cytokine removal *in vitro* (**Figure 3D,E**). These findings
284 confirm that MDNP can sequester pro-inflammatory cytokines to mitigate inflammatory
285 responses.
286 The innate immune responses that are triggered by LPS are mediated by Toll-like
287 receptor (TLR)-4 and subsequent activation of the transcription factors nuclear factor
288 kappa B (NF-κB) and activator protein 1 (AP-1) (Nyati et al., 2017). Upon encountering
289 various PAMPs and DAMPs, macrophages undergo rapid activation and secrete a
290 diverse range of cytokines and chemokines including IL-6 and TNF-α (Liu et al., 2017).
291 In this experiment, RAW-Blue cells, a NF-κB macrophage reporter cell line that releases
292 secreted alkaline phosphatase (SEAP) after activation, were used to gauge MDNP-
293 mediated effects following LPS stimulation (**Figure 3F**). The expression of IL-6 is tightly
294 regulated at multiple levels, including gene transcription, mRNA translation and mRNA
295 degradation levels. Furthermore, NF-κB activation was examined by exposing LPS-
296 activated RAW-Blue cells to 100 µg/mL MDNP for 1 hr (**Figure 3G**). PLGA was used as
297 a control and were unable to reduce NF-κB activation. The results demonstrate a
298 significant decrease in NF-κB activity, suggesting that MDNP possess the capacity to
299 mitigate pro-inflammatory cell signaling and reduce macrophage activation.
300
301 ***In vivo* biodistribution and anti-inflammatory effects of MDNP**
302 For the *in vivo* biodistribution study, MDNP were labeled with Cy5.5 and
303 administered intraperitoneally (IP) or intravenously (IV) into LPS-challenged mice (5
304 mg/kg LPS dose) twice at an MDNP dose of 2 mg/injection at 0.5 and 2 hr (**Figure 4A**).
305 At 4 hr, mice were euthanized to image the biodistribution of Cy5.5-MDNP in different
306 organs including liver, spleen, heart, kidney, and lung with an *in vivo* imaging system
307 (IVIS). Most of the Cy5.5-labeled MDNP were delivered to the liver and kidney by both
308 IP and IV injection, and very low amounts were detected in the spleen, heart, and lung
309 (**Figure 4B, C**).
310 We also investigated how the route of administration (IP versus IV) affected the
311 *in vivo* therapeutic effects in mice. Mice were challenged with 5 mg/kg LPS IP followed
312 by treatment with 2 mg MDNP at 0.5 hr and 2 hr post-LPS treatment. After 4 hrs, mice
313 were euthanized to collect organs samples and plasma (**Figure 4A**). Plasma samples
314 were processed using a MAGPIX Luminex multiplexing immunoassay system. This
315 system was employed to analyze the expression level of a 7-plex panel of pro-
316 inflammatory cytokines which included IL-6, TNF-α, MCP-1, IL-10, IL-1β, IFN-β, and
317 GROα. The heatmap demonstrates overall reduction of pro-inflammatory cytokines for
318 both routes (**Figure 4D**). The analysis revealed a significant reduction in IL-6 level
319 following both administration routes (**Figure 4E**), and a notable reduction in TNF-
320 α, MCP-1, and GROα for IP administered MDNP (**Figure 4F-K**). IV administration of
321 MDNP also reduced systemic cytokine levels, however it was slightly less effective. We
322 further evaluated blood biochemistry of albumin, alanine transaminase, creatine,

aspartate transferase, globulin, total protein, and blood urea nitrogen. Although minor reductions were observed for MDNP-treated mice, there was no significant alteration in levels of blood biochemistry parameters compared to LPS-treated controls (**Supplementary Figure S7**). The non-significant reductions in blood biochemistry following MDNP-treatment could be due to the pre-established severe inflammatory response, that could not be completely reversed by the endpoint of the study.

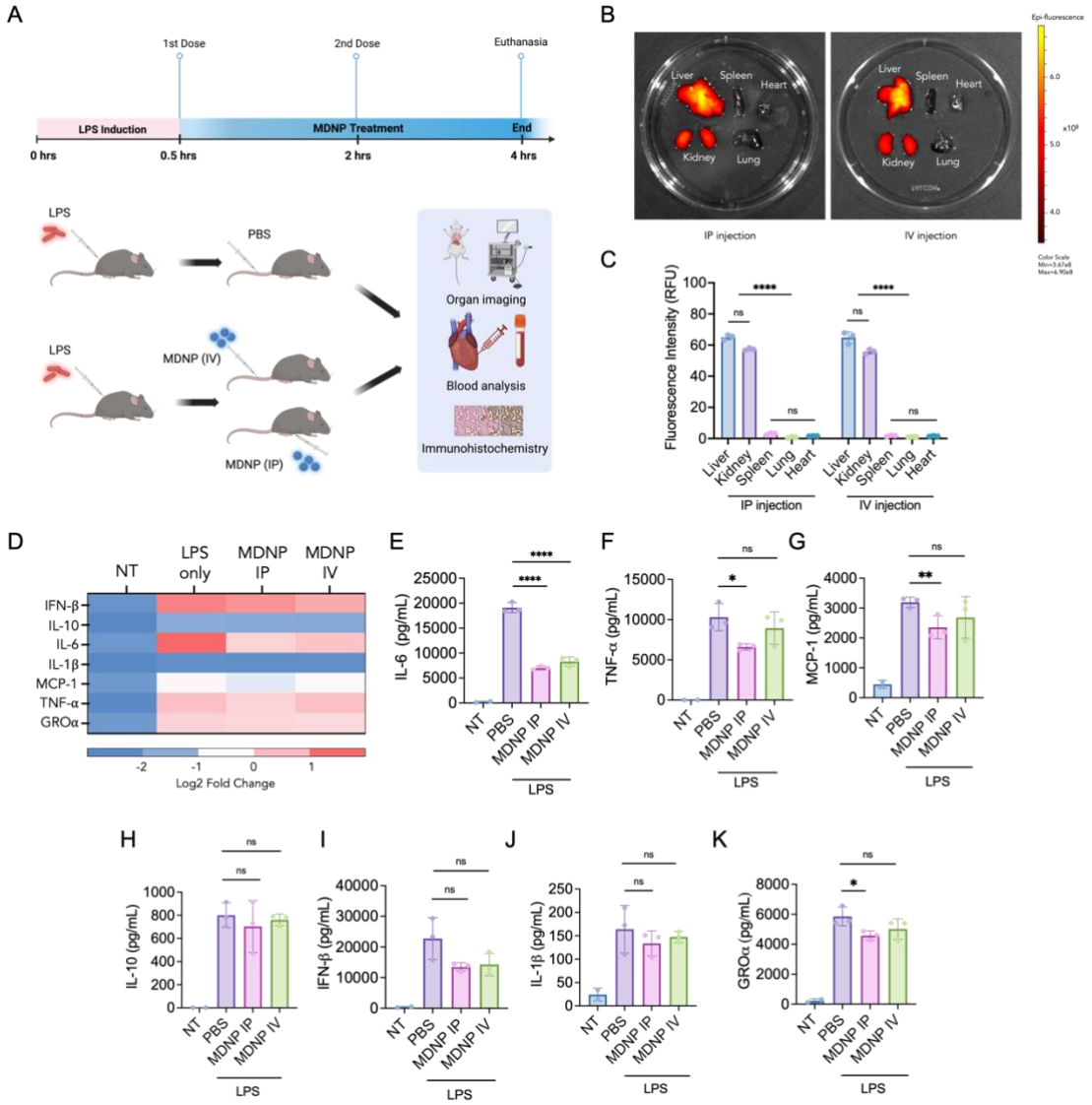

Figure 4. Route of administration biodistribution and anti-inflammatory effects of MDNP (A) Timeline of MDNP treatments following LPS challenge. The schematic illustrates the IP and IV injection performed on randomly selected C57BL/6J mice groups (LPS only, LPS+IP injection, and LPS+IV injection, n=3 per group). (B) Biodistribution of fluorescently labeled MDNP in mouse organs (liver, kidney, spleen, lung, and heart). (C) Fluorescence intensity measurement of MDNP biodistribution. (D) Heatmap of pro-inflammatory cytokine expression including: (E) IL-6, (F) TNF-α, (G) MCP-1, (H) IL-10, (I) IL-1β, (J) IFN-β, (K) GROα from mice plasma samples. Data are expressed as mean ± SD (n=3). *P<0.05, **p<0.05, ***p<0.005, and ****p<0.0005 versus PBS control group.

Treatment of MDNP accelerated organ recovery and improved survival

Histological analysis was used to evaluate the level of inflammation in tissues isolated from experiments conducted in **Figure 4**. H&E staining of five different organs including liver, kidney, spleen, lung, and heart are shown in **Figure 5**. LPS-treated liver showed severe immune cell infiltration, tubular necrosis was detected in the kidney, focal necrosis, and dysregulation in white pulp of spleen was observed, and extensive clots in the alveoli of lung appeared, but no significance of heart injury was measured. On the contrary, the IV and IP administered MDNP groups displayed notable improvements in histology scores when compared to the LPS group (**Figure 5B-F**). Based on the overall safety profile and reductions in pro-inflammatory cytokines, MDNP were used to further evaluate survival *in vivo*. Mice were challenged with lethal dose of 20 mg/kg LPS in sterile PBS intraperitoneally. Then, mice were monitored after two doses of 2 mg MDNP

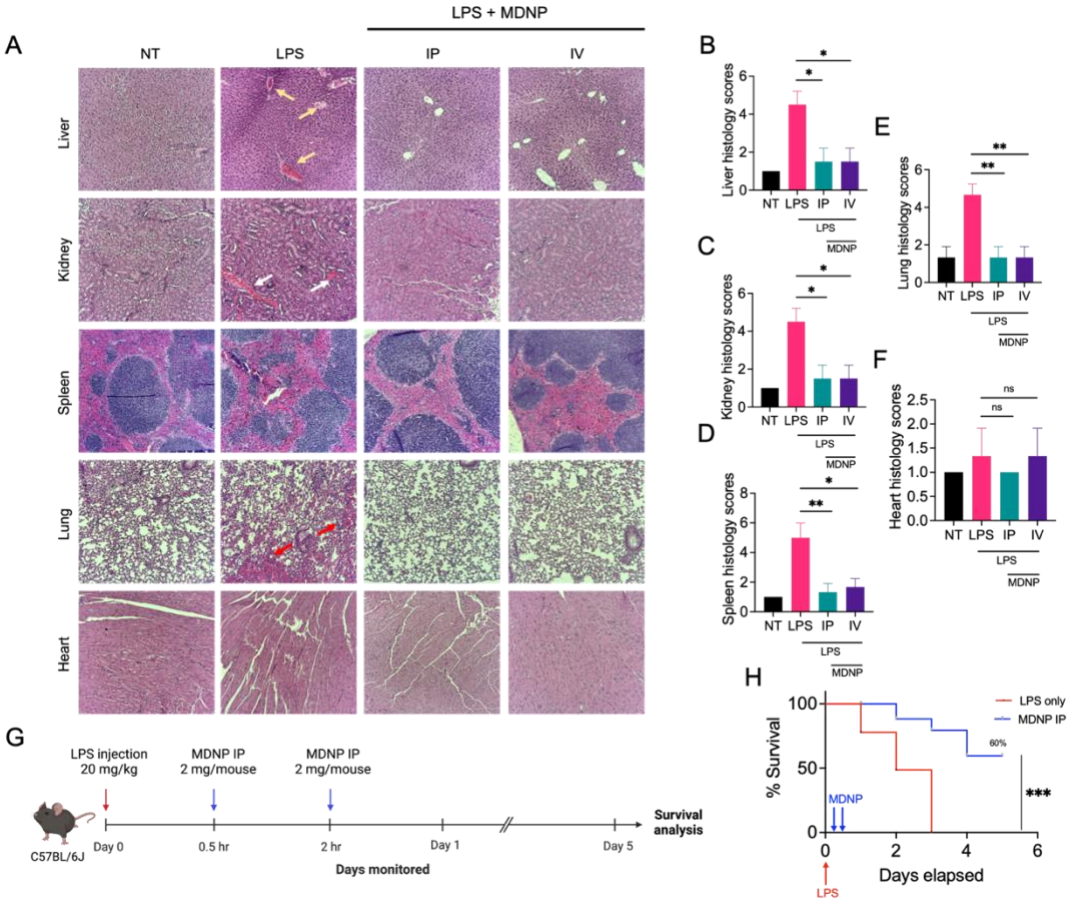

Figure 5. Representative images of organ recovery and survival effect by treatment of MDNP during LPS-induced sepsis. (A) H&E staining of liver, kidney, spleen, lung, and heart. The LPS treated group images shows presence of neutrophil infiltration (yellow arrow) in liver, tubular necrosis (white arrow) in the tubules in kidney, focal necrosis and dysregulation in white pulp of spleen, appearance of extensive clots (red arrow) in the alveoli in lungs, while no noticeable damage in heart. On the contrary, mice organs administered with IP and IV displayed notably reduced level of organ damage of organ damage. (B-F) Quantification of H&E staining. Levels of injury scores were calculated. Data are expressed as mean ± SD (n=3). *P<0.05, **p<0.05 versus LPS control group. (G) A schematic of survival study of LPS-treated and LPS+MDNP-treated C57BL/6J mice (n=10/group). (H) The survival analysis graph displays a significant difference between LPS only and the MDNP treatment group. Kaplan-Meier curves and a log-rank test was performed to compare the survival rates. ***p<0.0005.

341 (**Figure 5G**). As a result, 60% of MDNP treated mice survived, whereas 0% of the LPS
342 treated (control) mice survived (**Figure 5H**).
343
344 **Proteomic profiling of MDNP protein corona**
345 The ability of MDNP to reduce systemic cytokines and promote LPS mouse
346 survival prompted an exploration of the composition and types of proteins sequestered
347 by the MDNP. Adsorbed proteins were characterized by forming a protein corona on
348 MDNP *ex vivo* by incubating with either healthy or LPS-treated mouse plasma (MDNP-H
349 or MDNP-LPS, respectively) (**Figure 6A**). Proteomics analysis of these coronas
350 identified 297 total proteins (**Supplementary Table S1**), with 270 common between the
351 two conditions, 1 distinctive for healthy, and 26 for LPS-treated (**Figure 6B**). **Table 1**
352 presents a list of uniquely adsorbed proteins from each group. Among these, CD14,
353 LCN2 (lipocalin-2), APCS (Serum Amyloid P component), FABP4 (Fatty Acid Binding
354 Protein 4), NGP (Neutrophilic Granule Protein), and HSP90AA (Heat Shock Protein 90
355 alpha) are known to play roles in inflammation and categorized as APP excluding NGP.
356 The heatmap in **Figure 6C** shows the differential expression of total 297 detected
357 proteins. Comparing MDNP-H to MDNP-LPS, highlighted significant changes in protein
358 abundance, with 49 proteins being significantly upregulated and 100 proteins
359 downregulated (**Figure 6D**). Haptoglobin (Hp), which is known for its pro-inflammatory
360 properties(Shen et al., 2011), was found to be the most differentially abundant protein in
361 the MDNP-LPS corona. The top 15 proteins (over 20-fold change) identified in the
362 MDNP-LPS group are shown in **Supplementary Figure S8**. Among these, Hp,
363 Seprina3n, and Saa1 are well-known for their pro-inflammatory roles in regulating
364 inflammatory process and promoting the release of inflammation cytokines. Their levels
365 can increase dramatically during inflammation(Massart et al., 2020). **Figure 6E** lists the
366 canonical pathways of MDNP-LPS coronas from ingenuity pathway analysis (IPA). APR
367 signaling was most highly associated with MDNP-LPS corona. The network diagram in
368 **Figure 6F** illustrates the complex but close interaction of APP and these upstream pro-
369 inflammatory regulators within the APR signaling pathway. The highlighted connections
370 between APR shows its direct interaction with the APP sequestered on MDNP-LPS
371 coronas (Hp, Saa1, SerpinA3N) and a subset of upstream regulators (IL-6, TNF, IL1B,
372 AGT, HNF1A). Importantly, IL-6, TNF and IL1B play pivotal roles in either indirectly or
373 directly activating these APP. **Figure 6G** illustrates the result of *ex vivo* cytokine
374 sequestration assays using MDNP. It demonstrates that MDNP retains the ability to bind
375 and remove pro-inflammatory cytokines, such as IL-6 and TNF-α, from the LPS plasma.
376 It is also important to point out that protein corona formed on the surface of MDNP did
377 not activate any pro-inflammatory responses when treated on BMDM, supporting that
378 the formation of the corona effectively neutralizes the pro-inflammatory responses of
379 these various mediators (**Supplementary Figure S9**). **Figure 6H** summarizes the
380 proposed mechanism of MDNP by forming a multimodal protein corona comprised of

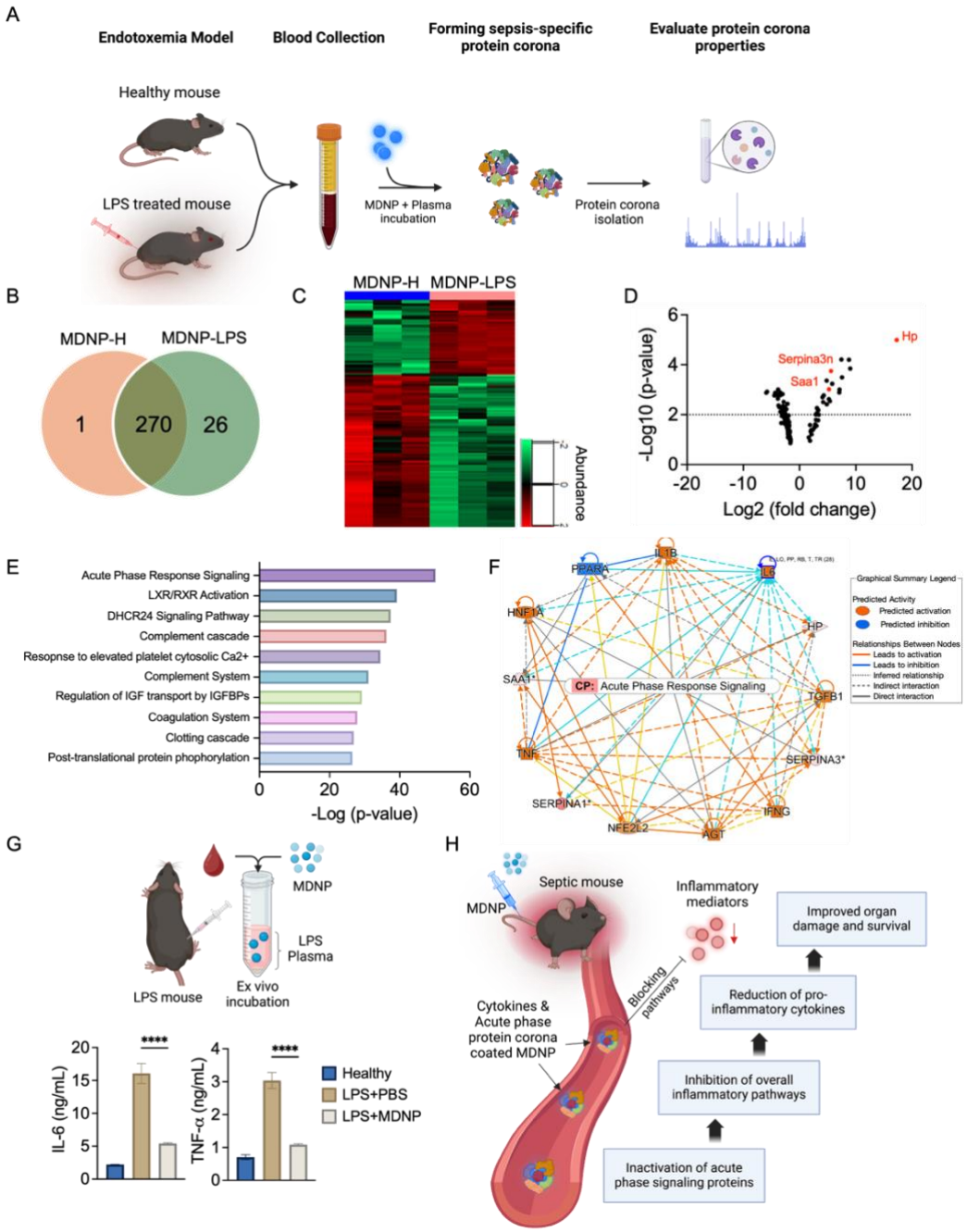

Figure 6. Mapping and identification of protein corona adsorbed onto the surface of MDNP. (A) A schematic showing the process of evaluating the MDNP protein corona. (B) Venn diagram illustrating a total of 296 proteins detected including unique (1 in healthy and 26 in LPS) and 270 shared proteins in the coronas. (C) Heatmap shows abundance of 49 upregulated and 100 downregulated proteins in MDNP-LPS group compared to MDNP-H healthy group. (D) Volcano plot of significantly upregulated and downregulated corona proteins. Hp, Serpina3n and Saa1 (red dots) are categorized as pro-inflammatory and acute phase response signaling proteins. (E) Top 10 canonical pathways associated with the significantly upregulated protein corona were identified, with acute phase response signaling being the most prominent pathway. (F) A network representation of acute phase response signaling proteins and major upstream regulators. (G) *Ex vivo* sequestration of pro-inflammatory cytokines by incubating LPS plasma with MDNP. Both IL-6 and TNF-α was significantly reduced by 8 hr treatment. (H) A graphical summary illustrating how the cytokine and acute phase protein corona-coated MDNP sequesters and neutralizes inflammatory proteins, thereby reducing overall inflammation.

382 pro-inflammatory cytokines and APP and neutralization. This inhibits the key
383 inflammatory pathways, blocking the production of pro-inflammatory upstream
384 regulators, ultimately reducing pro-inflammatory cytokines, improving organ function,
385 and increasing survival.
386
387 **MDNP treatment improved survival in polymicrobial sepsis model**

388 The survival benefit of MDNP was also tested in a clinically relevant severe
389 polymicrobial cecal ligation and puncture (CLP) sepsis model (**Figure 7A**). Mice
390 underwent the CLP procedure and were treated with three doses of 2 mg MDNP,
391 followed by monitoring for 5 days. To confirm MDNP could sequester pro-inflammatory
392 cytokines in CLP plasma, we first incubated MDNP with plasma isolated at 3 hr post-
393 CLP and observed an almost complete reduction in IL-6 and TNF-α (**Figure 7B**). In the
394 survival study, MDNP treated mice showed significant improvement in survival (40%)
395 compared to control group (0%) (**Figure 7C**). Taken together, the ability of MDNP to

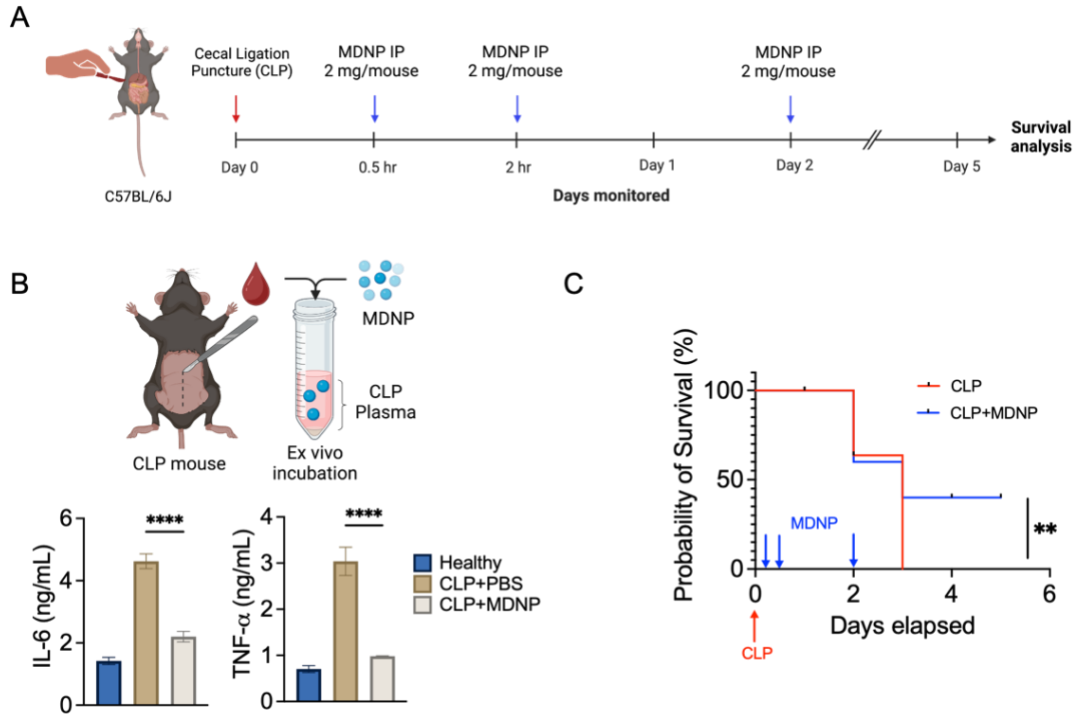

Figure 7. Survival effects of MDNP treatment on severe CLP model. (A) Schematic timeline of survival study of cecal ligation and puncture (CLP) C57BL/6J murine model with MDNP treatment (n=5/group) based on the complement cascade pathway from proteomics. Mice underwent CLP surgery to induce severe polymicrobial inflammation and three separate doses of MDNP were administered intraperitoneally (0.5, 2, 24 hr timepoint, 2 mg/injection) to analyze survival. (B) *Ex vivo* sequestration test of CLP plasma and MDNP showed that both IL-6 and TNF-α was significantly reduced. Kaplan-Meier curves and a log-rank test was performed to compare the survival rates. (C) The survival test displayed a significant improvement (40%) by the treatment of MDNP **p< 0.005. Data are expressed as mean ± SD (n=5). ****p<0.0005 versus PBS control group.

396 increase the survival of septic mice in the absence of antibiotics, highlights their
397 translational potential for treating inflammatory diseases, including sepsis.
398
399 **Discussion**
400 A tremendous amount of research has been implemented to enhance the clinical
401 management of inflammatory diseases caused by excessive stress (Miller and Raison,
402 2016), infections(Ikoba et al., 2015), autoimmune disorders (Miller et al., 2007), or
403 secondary diseases (Dufour et al., 2022). Despite many clinical trials aimed at blocking
404 specific inflammatory mediators, most have been unsuccessful due to the complexity
405 and multifactorial nature of inflammatory diseases. This highlights the need for
406 multimodal approaches that target multiple inflammatory mediators simultaneously to
407 improve treatment outcomes. The core pathophysiology of sepsis is known to involve
408 the disruption of the finely tuned balance between inflammatory and anti-inflammatory
409 immune responses (Jarczak et al., 2021). Recognition of pathogen- or damage-
410 associated molecular patterns (PAMPs/DAMPs) by innate immune cells functions as the
411 trigger to initiate inflammatory cell signaling and subsequent cytokine release, leading to
412 multiorgan damage, and death. Notably, studies have shown that increased plasma IL-6
413 and TNF-α levels in sepsis patients are correlated with mortality (Mera et al., 2011;
414 Unsinger et al., 2010; Wu et al., 2009). Our MDNP efficiently reduced systemic pro-
415 inflammatory cytokines including IL-6, TNF-α, among others (**Figure 4E, 6G, 7B**), while
416 simultaneously neutralizing additional pro-inflammatory mediators (APP) (**Figure 6D**).
417 Strategies for reducing pro-inflammatory mediators include conventional adsorption
418 resins like Cytosorb®, or more sophisticated membrane-coated nanoparticles
419 (Thamphiwatana et al., 2017), telodendrimer nanotraps (Shi et al., 2020), or abiotic
420 histone-capturing hydrogel nanoparticles (Koide et al., 2021b). Although these
421 approaches have shown success in certain cases, the complex structural composition
422 and manufacturing processes may hinder rapid development. In contrast, we developed
423 a MDNP, isolated from maca root, as a novel approach to mitigate broad pro-
424 inflammatory responses from abundant and readily available plant material, facilitating
425 convenient access, and long-term storage potential (**Figure 1**). We further
426 demonstrated their ability to reduce organ damage and improve survival as reflected in
427 two representative and lethal sepsis models (**Figure 5A, 5H, 7C**) through the formation
428 of a multimodal protein corona (**Figure 6**).
429 Sepsis endotypes include hyperinflammatory (early) and immunosuppressive
430 (late) states (Hotchkiss et al., 2013). A clinical study indicated that early-identified sepsis
431 is associated clinically with higher mortality than late-identified sepsis (Jee et al., 2020).
432 Thus, achieving control over the cytokine storm holds great potential to improve patient
433 survival. Modes of cytokine sequestration have generally relied on charge-based
434 interactions, where most pro-inflammatory cytokines are negatively charged, and anti-
435 inflammatory cytokines are positively charged at neutral pH (Messina et al., 2024).

436 Interestingly, the zeta potential of MDNP was -9.6 mV (**Figure 1E**), yet cytokines like IL-
437 6 (pI 6.96) and TNF-α (pI 5.01) were strongly sequestered but IL-1β (pI 4.96) and IFN-γ
438 (pI 8.25) were not (**Figure 2K, L, S6**). These differences suggest the possibility of a
439 combination of forces driving the binding of cytokines to the surface of MDNP. Our
440 lipidomics analysis of MDNP (**Figure 1H, I**) showed the presence of multiple charged or
441 ionizable lipid species like Cer (Phyto), HexCer (Phyto), FFA, LPC, and PC
442 (**Supplementary Figure S2**). Therefore, it is possible that a combination of local charge
443 and hydrophobic interactions are contributing to the apparently selective sequestering of
444 specific pro-inflammatory cytokines. Although we have not fully elaborated how MDNP
445 facilitate a selective binding interaction for certain cytokines, which is a limitation of our
446 study, our results provide the basis for future studies to investigate the role of specific
447 lipid components and their ability to alter binding interactions.
448 Upon exposure to biological fluids, nanoparticles dynamically adsorb
449 biomolecules onto their surface, forming a protein corona that dictates how
450 nanoparticles interact with host cells. These interactions can alter both drug delivery
451 efficiency (Corbo et al., 2016) and biological function (Cedervall et al., 2007) of the
452 particles. The analysis of MDNP protein coronas revealed significant differences
453 between MDNP-H and MDNP-LPS groups, highlighting that unique protein fingerprints
454 are associated with MDNP under inflammatory conditions. This is consistent with the
455 concept of the 'personalized protein corona', which demonstrates that unique protein
456 fingerprints are formed on the surface of nanoparticles as a function of disease state (Ju
457 et al., 2020; Shaw and Pearson, 2022). The ability of MDNP to bind cytokines in LPS- or
458 CLP-treated mouse plasma confirmed its ability to directly modulate inflammatory
459 responses in a disease setting (**Figure 6G, 7B**). An unexpected finding from our
460 proteomics analysis was the identification of multiple pro-inflammatory APP being
461 upregulated in the coronas of MDNP-LPS like Hp, SerpinA3N, and Saa1 (**Figure 6D**).
462 Hp activates immune cells, promotes secretion of pro-inflammatory cytokines, and
463 interacts with complement system, potentially intensifying inflammatory responses
464 (Torres et al., 2022). SerpinA3N is involved in regulating inflammatory responses by
465 controlling protease activity to prevent excessive tissue damage, but it's upregulated
466 under inflammatory conditions (Liu et al., 2023). Saa1 plays direct role in recruiting
467 immune cells and modulating pro-inflammatory cytokines (Ye and Sun, 2015).
468 Supporting that MDNP neutralized the pro-inflammatory functions of corona
469 constituents, MDNP-LPS was cultured with BMDM and no significant increase in IL-6 or
470 TNF-α was detected (**Supplementary Figure S9**). These results highlighted that MDNP
471 formed multifaceted protein corona under inflammatory conditions that could mitigate
472 aberrant immune activation caused by individual components, representing a novel
473 approach to the treatment of inflammatory diseases.
474 Here, we demonstrated that MDNP sequestered and neutralized multiple pro-
475 inflammatory cytokines and APP in its protein corona to reveal a highly effective anti-

476 inflammatory plant-derived therapeutic strategy for managing severe inflammatory
477 responses. Our data indicates that MDNP exhibit negligible toxicity, are efficiently
478 internalized by macrophages, display immunomodulatory activities, and demonstrate
479 significant therapeutic efficacy. Administration of MDNP *via* IP or IV routes effectively
480 reduced pro-inflammatory cytokines and promoted improved survival in two
481 representative sepsis mouse models, LPS-induced endotoxemia and CLP polymicrobial
482 sepsis. This research underscores the broad therapeutic potential of the MDNP, which
483 leverages a unique and never previously examined mechanism of action through the
484 formation of a multimodal protein corona that effectively binds and neutralizes pro-
485 inflammatory cytokines and APP from propagating systemic inflammation.
486
487 **Materials and methods**
488 **Isolation, purification, and characterization of maca-derived lipid nanoparticles**
489 **(MDNP)**
490 A fine ground organic powder of 100% *Lepidium meyenii* Walp (maca) (Family:
491 Brassicaceae, Order: Brassicas) was purchased from an organic producer, Happy
492 Andes (https://www.happyandes-usa.com/). Maca powder (30 g) was mixed in 400 mL
493 of autoclaved deionized water and stirred for 12 hrs at room temperature to make maca
494 juice. The obtained maca juice was transferred to 50 mL tubes and centrifuged at 3,000
495 x g for 20 min at 20°C then the supernatant was centrifuged again in new 50 mL tubes
496 at 10,000 x g for 2 hrs at 20°C to remove small and large fibers. Next, the clear light
497 brown colored supernatant was collected in 70 mL polycarbonate ultracentrifuge bottles
498 (Beckman Coulter, Brea, CA) and was ultracentrifuged with using a 45 Ti rotor
499 (Beckman Coulter, Brea, CA) at 150,000 x g for 2 hrs at 4°C. Then, the collected pellets
500 were suspended in 2 mL of phosphate-buffered saline (PBS) through dispersion with an
501 ultrasonic processor. PBS-suspended maca pellets were transferred to a sucrose
502 gradient (8%, 20%, 35% [g/v]) and ultracentrifuged at 150,000 x g for 2 hrs at 4°C, then
503 the cloudy band between 8% and 20% sucrose was collected as previously described
504 (Sung et al., 2019). The concentration of MDNP was measured using a Bio-Rad
505 quantification assay. The quantified MDNP were stored at 4°C. The size and zeta
506 potential of MDNP was measured by dynamic light scattering (DLS) using a Zetasizer
507 Nano ZSP (Malvern, UK). MDNP were also tested under different storage temperature
508 conditions (room temperature (RT), 4°C, -20°C, and -80°C) to determine their stability.
509 Transmission electron microscopy (TEM) images of MDNP were acquired using a
510 formvar-coated copper grid and staining using 1% uranyl acetate. Differential Scanning
511 Calorimeter (DSC) 2500 (TA Instruments, New Castle, DE) was used to analyze the
512 temperature and heat flow associated with thermal transition in the MDNP. 5 µL of
513 sample in liquid form was added into a hermetic aluminum pan and sealed with metal lid
514 (DSC Consumables, Austin, MN) with Tzero sample press kit (TA Instruments, New
515 Castle, DE). The following thermal procedure was used to scan: ramp 2°C/min from

25°C to 80°C. The heat flow transition was analyzed on a plot by TA analysis software Trios (Version 5.4.0.300). For lyophilization, frozen MDNP in 1.5 mL tubes with holes on top of screw caps were placed in a benchtop freeze-dryer (Labconco, Kansas City, MO) overnight. Completely dried samples were collected and reconstituted in PBS for stability testing.

Lipid extraction and composition analysis

A total lipid extract was prepared using a modified methyl-tert-butyl ether (MTBE) lipid extraction protocol (Matyash et al., 2008). Briefly, 400 µL of cold methanol and 10 µL of internal standard mixture (EquiSPLASH lipidomix) were added to each sample followed by incubation at 4°C, 650 RPM shaking for 15 min. Next, 500 µL of cold MTBE was added followed by incubation at 4°C for 1 hr with 650 RPM shaking. 500 µL of cold water was added slowly and resulting extract was maintained 4°C, 650 rpm shaking for 15 min. Phase separation was completed by centrifugation at 8,000 RPM for 8 min at 4°C. The upper, organic phase was removed and set aside on ice. The bottom, aqueous phase was re-extracted with 200 µL of MTBE followed by 15 min of incubation at 4°C with 650 RPM shaking. Phase separation was completed by centrifugation at 8,000 RPM for 8 min at 4°C. The organic extract was dried under a steady stream of nitrogen at 30°C. The recovered lipids were reconstituted in 200 µL of chloroform:methanol (1:1, v/v) containing 200 µM of butylated hydroxytoluene. Prior to analysis, samples were further diluted with acetonitrile:isopropanol:water (1:2:1, v/v/v). The total lipid extract was analyzed by liquid chromatography coupled to high resolution tandem mass spectrometry (LC-MS/MS). The LC-MS/MS analyses were performed on an Agilent 1290 Infinity LC coupled to an Agilent 6560 Quadrupole Time-of-Flight (Q-TOF) mass spectrometer. The separation was achieved using a C18 CSH (1.7 µm; 2.1 x 100 mm) column (Waters, Milford, MA). Mobile phase A was 10 mM ammonium formate with 0.1% formic acid in water/acetonitrile (40:60, v/v) and mobile phase B was 10 mM ammonium formate with 0.1% formic acid in acetonitrile/isopropanol (10:90, v/v). The gradient was ramped from 40% to 43% B in 1 min, ramped to 50% in 0.1 min, ramped to 54% B in 4.9 min, ramped to 70% in 0.1 min, and ramped to 99% B in 2.9 min. The gradient was returned to initial conditions in 0.5 min and held for 1.6 min for column equilibration. The flow rate was 0.4 mL/min. The column was maintained at 55°C and the auto-sampler was kept at 5°C. A 2 µL injection was used for all samples. LC-MS data from the iterative MS/MS workflow was analyzed for lipid identification via Agilent's Lipid Annotator (version 1.0). Positive and negative ion mode adducts included $[M+H]^+$, $[M+Na]^+$, $[M+NH_4]^+$, $[M-H]^-$, and $[M+CH_3CO_2]^-$, respectively. The LC-MS data from the MS^1 workflow were processed using Agilent's MassHunter Profinder (version 10.0).

Characterization of MDNP protein composition and MDNP protein corona fingerprints in healthy and LPS plasma

To form the MDNP protein corona, purified MDNP were incubated with plasma isolated from healthy and LPS-treated C57BL/6J mice for 4 hrs at 37°C. MDNP bound to proteins were washed and centrifuged 3 times at 13,000 xg, 4°C with 1x cold PBS. Then it was evaluated using the below protocol. Prepared samples were lysed in a lysis buffer containing 5% sodium dodecyl sulfate (Sigma, St. Louis, MO), 50 mM triethylammonium bicarbonate (1M, pH 8.0) (Sigma, 7408). Proteins were extracted and digested using S-trap micro columns (ProtiFi, Farmingdale, NY). The eluted peptides from the S-trap column were dried, and peptide concentration was determined using a BCA assay kit (Thermo Fisher Scientific, 23275), after reconstitution in 0.1% formic acid. All tryptic peptides were separated on a nanoACQUITY Ultra-Performance Liquid Chromatography analytical column (BEH130 C18, 1.7 µm, 75 µm x 200 mm; Waters Corporation, Milford, MA, USA) over a 185-min linear acetonitrile gradient with 0.1% formic acid on a nanoACQUITY Ultra-Performance Liquid Chromatography system (Waters Corp, Milford, MA) and analyzed on a coupled Orbitrap Fusion Lumos Tribrid mass spectrometer (Thermo Scientific, San Jose, CA). Full scans were acquired at 240,000 resolutions, and precursors were fragmented by high-energy collisional dissociation at 35% for up to 3 sec. MS/MS raw files were processed using Thermo Proteome Discoverer (PD, version 3.0.0.757) with the Sequest HT search engine against the plant metagenome database and UniProt mouse reference proteome. Trypsin was used with a maximum of two missed cleavages, and peptide lengths were restricted to 6-144 amino acids. Label-free quantification was performed using the Minora feature detector. Protein identification was filtered at a 1% false discovery rate across PSM, peptide, and protein levels using the Percolator algorithm in PD. Exported protein abundances were analyzed with Perseus software (version 1.6.14.0), with further filtering to include only proteins identified without missing values across all samples. The quantitative protein data were $\log_2$ transformed and further normalized using median centering. Two-tailed student's t-test (adjusted p-value < 0.05) was applied to determine the differentially expressed proteins (DEPs). Plant data was analyzed with library from Uniprot and the Plant Proteome Database (Lepidium meyenii: taxonomy ID 153348, entry: 92 sequences; Plant metagenome: taxonomy ID 1297885, entry: 27312 sequences; Zingiberales: taxonomy ID 4618, entry: 357900) Ingenuity Pathway Analysis (Qiagen) was utilized to identify canonical pathways, biological function, upstream regulators and disease association.

Cell culture

The generation of bone marrow-derived macrophages (BMDM) followed a previously published method(Truong et al., 2024). As established, the tibia and femur from a C57BL/6J mouse was isolated by removing bulk muscles and connective

595 tissues. RPMI media (supplemented with L-glutamine, penicillin (100 units/mL),
596 streptomycin (100 µg/mL), 10% heat-inactivated FBS, and 20% L929 cell-conditioned
597 media) drawn needles were inserted into bones to flush the marrow into a 10 cm petri
598 dish. The collected bone marrow was filtered to grow in uncoated 10 cm cell culture
599 plates. BMDM were cultured in RPMI media conditioned with L929 at 37°C, 5% CO_2.
600 The media was replaced every 3 days. On Day 8-10, BMDM were lifted using Versene
601 (Gibco, Grand Island, NY), to be used for subsequent experiments. Trypan blue solution
602 was used to determine the cell number and viability with an EVE™ Automated Cell
603 Counter (NanoEntek, Waltham, MA). RAW-blue cells were also cultured to confluency in
604 75 cm^2 flasks in identical incubation condition with Dulbecco's Eagle Medium (DMEM)
605 supplemented with penicillin (100 U/mL), streptomycin (100 U/mL), and heat inactivated
606 fetal bovine serum (10%).
607
608 **Mice**
609 Male C57BL/6 (6 to 8-week-old) purchased from the Jackson Laboratory (Bar
610 Harbor, ME) were maintained in cages at ambient temperature, 55% relative humidity,
611 and under a 12 hr dark/light cycle. LPS-induced endotoxemia model: Mice were
612 challenged with 5 mg/kg LPS intraperitoneally (IP) prior to treatment with two doses of 2
613 mg MDNP at 30 min and 2 hr *via* both IP and intravenous (IV) injection. Cecal ligation
614 and punction (CLP) model: Mice were lightly anesthetized with a mixture of ketamine
615 (75 mg/kg) and xylazine (15 mg/kg) at 1:1 ratio. After abdominal fur was removed, a
616 small incision was made to expose the cecum. The cecum was then ligated with a silk
617 suture and perforated with 19-gauge needle. A small amount of feces was extruded by
618 gently squeezing the cecum, the cecum was replaced, and the abdomen was sutured
619 after the bowel was repositioned. Experimental groups were IP injected with three
620 doses of 2 mg MDNP at 30 min, 2 hr, and 24 hr timepoint. All experiments were
621 performed in compliance with the protocol by the University of Maryland, Baltimore
622 Institutional Animal Care and Use Committee (IACUC) as well as the ARRIVE
623 guidelines.
624
625 **Cytotoxicity assay**
626 To measure the cytotoxicity of MDNP, a PI/Annexin V-FITC apoptosis assay was
627 conducted using BMDM. The assay utilizes propidium iodide (PI) staining to distinguish
628 between early and late-stage apoptotic cells. FITC labeling allow for the visualization of
629 Annexin V-bound cells using flow cytometry. Cultured BMDM at a density of 1.0 x 10^5
630 per well were treated with MDNP at 1 mg/mL for 8 hrs, then the cells were harvested
631 with Versene after washing with PBS. Collected cells were centrifuged at 500 x g for 5
632 min and cell pellets were resuspended in 1x binding buffer. 100 µL of cell suspension in
633 flow cytometry tubes were added with Annexin V-FITC and PI to be analyzed by flow

634 cytometry. The data was analyzed by De Novo software FCS Express 7 (Dotmatics,
635 Boston, MA).
636
637 ***In vitro* cellular internalization**
638 BMDM were seeded overnight in Falcon Culture slides at a density of 0.5 x 10^5
639 per well. Cy5.5 was incubated with MDNP under shaking for 30 min in the dark to label
640 the MDNP and excessive Cy5.5 dye was removed by 20 min centrifugation at 13,000 x
641 g prior to use. Then, 50 µL of Cy5.5-labled MDNP were added to 0.5 mL of culture
642 medium and incubated with cells for 0, 4, 8 hrs. Negative control, untreated cells were
643 used to establish the 0 hr timepoint. At the determined timepoints, cells were washed
644 with PBS three times, fixed with 4% paraformaldehyde (PFA) for 10 min, and
645 dehydrated with acetone for 5 min at -20°C. After blocking the culture with 1% BSA in 1x
646 PBS 30 min, the cells were washed again with 1x PBS and treated with 100 µL of
647 fluorescein isothiocyanate (FITC)-labeled phalloidin (1:50 dilution in PBS) for 30 min to
648 stain F-actin. The cells were then washed two times with 1x PBS and dried in the dark
649 condition and glass cover slips were mounted with mounting medium containing 4',6-
650 diamidino-2-phenylindole (DAPI) after carefully removing the plastic chambers. The final
651 fluorescence images were captured using an Olympus fluorescence microscope (Tokyo,
652 Japan) equipped with Hamamatsu Digital Camera ORCA-03G and Nikon software was
653 used to analyze the image data.
654
655 **Flow cytometric phenotyping of MDNP-treated macrophages**
656 BMDM were seeded at a density of 1.0 x 10^5 per well were in a sterile 24 well
657 plate. Cells were treated with 100 ng/mL of LPS in complete media for 24 hrs to induce
658 inflammation. Then, 100 µg/mL and 200 µg/mL MDNP was treated for 8 hrs. Cells were
659 resuspended in MACS buffer (PBS pH 7.2 supplemented with 1% FBS and 0.4% 0.5 M
660 EDTA, Quality Biological, Gaithersburg, MD) and transferred to the flow cytometry
661 tubes. FcR blocking (CD16/32, Biolegend, San Diego, CA) was performed and cells
662 were stained with following surface marker antibodies: Live/Dead fixable green, F4/80,
663 CD11b, MHCII, CD206, CD80, and CD86 (Biolegend, San Diego, CA). Samples were
664 analyzed using Cytek Aurora 3 (Fremont, CA). FCS Expression 7 Flow Cytometry De
665 Novo Software was used for flow data processing. Mean fluorescence intensity (MFI)
666 was generated by GraphPad Prism Software 10.1.1.
667
668 ***In vitro* pro-inflammatory cytokine sequestration and effects on NF-κB activity**
669 Anti-inflammatory properties of MDNP were investigated in two ways;
670 prophylactic and therapeutic. For prophylactic treatment, BMDM at a density of 1.0 x
671 10^5 per well were treated with 100 µg/mL MDNP for 8 hrs and 100 ng/mL of LPS in
672 complete media in 24 well plates (Corning, Corning, NY) were incubated for 4 hrs. For
673 therapeutic study, BMDM in identical culture condition as above were treated with 100

674 ng/mL of LPS for 4 hrs and 100 μg/mL of MDNP was subsequently added and
675 incubated for 8 hrs. Supernatants were then collected to measure the reduction of pro-
676 inflammatory cytokines including IL-6, TNF-α, IL-1β, and IFN-γ by enzyme-linked
677 immunosorbent assay (ELISA) (BioLegend, San Diego, CA). We also assessed the
678 ability of MDNP to modulate cytokine levels in the absence of cells. The supernatants
679 from another set of LPS-treated BMDM were collected and incubated with 100 μg/mL of
680 MDNP in a time dependent manner (0, 0.5, 1, 4, 8, 12, and 24 hrs). Lastly, we confirmed
681 the direct ability of MDNP to sequester IL-6 by incubating 5 ng/mL of IL-6 recombinant
682 protein in DMEM with 100 μg/mL of MDNP for 8 hrs. Remaining IL-6 levels were
683 measured using ELISA.
684 An NF-κB reporter cell line, RAW-Blue, was used to determine the ability of
685 MDNP to alter NF-κB activity due to LPS stimulation. The cells were plated at a density
686 of 1.0 x 10^5 per well and were stimulated with LPS for 4 hrs and treated with 100 μg/mL
687 MDNP for 8 hrs. Then, QUANTI-Blue was added to the collected supernatant in flat
688 bottom 96 well plate. It was incubated at 37ºC for 1 hr, then secreted embryonic alkaline
689 phosphatase (SEAP) reporter was detected using a spectrophotometer at 620-655 nm.
690 Poly(lactic-co-glycolic acid) (PLGA) particles of similar size as MDNP were used as a
691 control and fabricated using a microfluidics device as we previously described(Truong et
692 al., 2021). The size and zeta potential of the PLGA was measured 163.8 nm and -39.3
693 mV, respectively.
694
695 ***Ex vivo* cytokine sequestration assay**
696 To evaluate the cytokine sequestration ability of MDNP in mouse plasma *ex vivo*,
697 100 μg/mL of MDNP in PBS was prepared and added to 100 μL of diluted LPS-treated
698 or CLP mouse plasma to ultracentrifuge tubes. The mixture tubes were incubated at
699 37ºC for 8 hrs. After incubation, samples were centrifuged at 2,000 x g for 10 min to
700 pellet the cytokine bound MDNP. Then the supernatant was collected to measure IL-6
701 and TNF-α levels using ELISA (Biolegend, San Diego, CA).
702
703 ***In vivo* biodistribution and anti-inflammatory effect following LPS challenge**
704 The *in vivo* biodistribution study was performed by intraperitoneal (IP) or
705 intravenous (IV) injection of MDNP that were labeled with the near-infrared fluorescent
706 Cy5.5 dye. Mice were administered 2 mg of Cy5.5-MDNP twice (0.5 and 2 hr time
707 point)-post LPS challenge (5 mg/kg) and euthanized after 4 hrs to collect blood by
708 cardiac puncture and organs including liver, lung, spleen, heart, and kidneys. The
709 fluorescence of the organs was imaged using an *in vivo* imaging system (IVIS) with
710 emission (720 nm) upon laser excitation (675 nm). Blood samples were centrifuged at
711 1,000 x g for 20 min at 4°C in microtainer capillary blood collection plasma tubes. The
712 plasma samples were used to measure the alteration of systematic cytokines levels
713 using a Luminex MAGPIX System (Luminex, Austin, TX). The 7-plex panel included

714 murine IL-6, TNF-α, MCP-1, IL-10, IL-1β, IFN-β, and IFN-γ. Blood biochemistry was also
715 measured for alanine aminotransferase (ATL/SGPT), aspartate aminotransferase
716 (AST/SGOT), creatine (CREA), blood urea nitrogen (BUN), total protein (TP), and
717 globulin, and albumin (VRL Animal Health Diagnostics, Gaithersburg, MD). The
718 collected organs were fixed in 4% formalin immediately after euthanasia and paraffin-
719 embedded for sectioning. Hematoxylin & eosin (H&E) staining was performed using
720 standard procedures by the Pathology Biorepository Shared Services Core at the
721 University of Maryland, Baltimore. The level of injury scores was calculated based on
722 the scoring criteria: score 0, no damage; score 1, >10% slight inflammation; score 2, 10-
723 25% mild; score 3, 26-50% moderate; score 4, 51-75% severe; score 5, >75% necrosis.
724
725 ***In vivo* sepsis survival study**
726 The *in vivo* survival study was carried out using two representative sepsis
727 models: a lethal LPS-induced endotoxemia and CLP polymicrobial mouse model. For
728 endotoxemia, C57BL/6J mice were challenged with 20 mg/kg LPS and two doses
729 MDNP (2 mg) administered *via* IP injection. For CLP model, the cecum of anesthetized
730 C57BL/6J mice was perforated to release fecal materials into peritoneal cavity to
731 generate an exacerbated polymicrobial infection. Three doses of MDNP (2 mg/injection)
732 were administered via IP route. Survival for each model was evaluated over the course
733 of 5 days. Body temperature was also recorded every day for CLP mice.
734
735 **Statistical analysis**
736 Data evaluation was performed using GraphPad Prism Software 10.1.1 (San
737 Diego, CA). One-way ANOVA and t-test for unpaired data were employed to evaluate
738 statistical significance along with Tukey's multiple comparison test. Kaplan-Meier
739 survival curve and statistical significance of mouse survival were determined with a
740 long-rank (Mantel-Cox) X^2 test. Significant differences were indicated as $p<0.05$,
741 $p<0.005$, $p<0.0005$ related to control unless otherwise stated.
742
743 **Data availability statement**
744 All lipidomics and proteomics raw data are included in the supporting information.
745 Additional datasets supporting the findings are available upon reasonable request from
746 the corresponding author.
747
748 **Acknowledgements**
749 This work was supported by Startup funds from the University of Maryland
750 School of Pharmacy, the National Institute of General Medical Sciences of the National
751 Institute of Health under Award number R35GM142752 awarded to R.M.P. A.L.C. was
752 supported by a pharmaceutical sciences (PSC) departmental fellowship. This
753 publication was supported by funds through the Maryland Department of Health's
754 Cigarette Restitution Fund Program and the National Cancer Institute – Cancer Center

Support Grant (CCSG) – P30CA134274. University of Maryland School of Medicine's & Greenebaum Comprehensive Cancer Center's Flow Cytometry Core–Baltimore, Maryland. University of Maryland School of Medicine's Center for Translational Research in Imaging – Baltimore, Maryland. University of Maryland School of Pharmacy Mass Spectrometry Center (SOP1841-IQB2014). BioRender was used for preparing graphics. The content is solely the responsibility of the authors and does not necessarily represent the official view of the National Institutes of Health.

Author contributions

Junsik J. Sung: Conceptualization, Formal analysis, Investigation, Methodology, Visualization, Writing – original draft, Writing – review & editing. **Jacob R. Shaw:** Methodology, Writing – review & editing. **Josie D. Rezende:** Investigation, Methodology. **Shruti Dharmaraj:** Investigation, Methodology. **Andrea L. Cottingham:** Investigation, Methodology. **Mehari M. Weldemariam:** Investigation, Methodology. **Jace W. Jones:** Investigation, Methodology, Resources, Supervision. **Maureen A. Kane:** Investigation, Methodology, Resources, Supervision. **Ryan M. Pearson:** Conceptualization, Funding acquisition, Methodology, Resources, Supervision, Writing – original draft, Writing – review & editing.

Declaration of interests

J.J.S. and R.M.P are inventors on a patent application that describes the isolation and use of MDNP for the treatment of inflammatory diseases.

780 **References**

781 Ansar, W., Ghosh, S., 2016. Inflammation and Inflammatory Diseases, Markers, and
782 Mediators: Role of CRP in Some Inflammatory Diseases, in: Ansar, W., Ghosh, S.
783 (Eds.), Biology of C Reactive Protein in Health and Disease. Springer India, New
784 Delhi, pp. 67–107.

785 Cao, F., Zhang, H., Yan, Y., Chang, Y., Ma, J., 2023. Extraction of polysaccharides from
786 Maca enhances the treatment effect of 5-FU by regulating CD4+T cells. Heliyon 9,
787 e16495.

788 Castellheim, A., Brekke, O.-L., Espevik, T., Harboe, M., Mollnes, T.E., 2009. Innate
789 Immune Responses to Danger Signals in Systemic Inflammatory Response
790 Syndrome and Sepsis. Scand J Immunol 69, 479–491.

791 Cedervall, T., Lynch, I., Lindman, S., Berggård, T., Thulin, E., Nilsson, H., Dawson, K.A.,
792 Linse, S., 2007. Understanding the nanoparticle–protein corona using methods to
793 quantify exchange rates and affinities of proteins for nanoparticles. Proc Natl Acad
794 Sci 104, 2050–2055.

795 Chafe, S.C., 1969. The fine structure of the collenchyma cell wall. Planta 90, 12–21.

796 Chen, L., Deng, H., Cui, H., Fang, J., Zuo, Z., Deng, J., Li, Y., Wang, X., Zhao, L., 2018.
797 Inflammatory responses and inflammation-associated diseases in organs.
798 Oncotarget 9, 7204–7218.

799 Corbo, C., Molinaro, R., Parodi, A., Toledano Furman, N.E., Salvatore, F., Tasciotti, E.,
800 2016. The Impact of Nanoparticle Protein Corona on Cytotoxicity, Immunotoxicity
801 and Target Drug Delivery. Nanomedicine 11, 81–100.

802 Dufour, J.-F., Anstee, Q.M., Bugianesi, E., Harrison, S., Loomba, R., Paradis, V., Tilg,
803 H., Wong, V.W.-S., Zelber-sagi, S., 2022. Current therapies and new developments
804 in NASH. Gut 71, 2123.
805 Ehlting, C., Wolf, S.D., Bode, J.G., 2021. Acute-phase protein synthesis: a key feature
806 of innate immune functions of the liver. Biol Chem 402, 1129–1145.
807 Fang, X., Feng, J., Zhu, X., Feng, D., Zheng, L., 2024. Plant-derived vesicle-like
808 nanoparticles: A new tool for inflammatory bowel disease and colitis-associated
809 cancer treatment. Mol Ther 32, 890–909.
810 Fei, W., Hou, Y., Yue, N., Zhou, X., Wang, Y., Wang, L., Li, A., Zhang, J., 2020. The
811 effects of aqueous extract of Maca on energy metabolism and immunoregulation.
812 Eur J Med Res 25, 24.
813 Fei, W., Zhang, J., Yu, S., Yue, N., Ye, D., Zhu, Y., Tao, R., Chen, Yan, Chen, Yawen, Li,
814 A., Wang, L., 2022. Antioxidative and Energy Metabolism-Improving Effects of
815 Maca Polysaccharide on Cyclophosphamide-Induced Hepatotoxicity Mice via
816 Metabolomic Analysis and Keap1-Nrf2 Pathway. Nutrients 14.
817 Hirano, T., 2021. IL-6 in inflammation, autoimmunity and cancer. Int Immunol 33, 127–
818 148.
819 Hotchkiss, R.S., Monneret, G., Payen, D., 2013. Sepsis-induced immunosuppression:
820 from cellular dysfunctions to immunotherapy. Nat Rev Immunol 13, 862–874.
821 Ikoba, U., Peng, H., Li, H., Miller, C., Yu, C., Wang, Q., 2015. Nanocarriers in therapy of
822 infectious and inflammatory diseases. Nanoscale 7, 4291–4305.
823 Jarczak, D., Kluge, S., Nierhaus, A., 2021. Sepsis—Pathophysiology and Therapeutic
824 Concepts. Front Med (Lausanne) 8.

825 Jee, W., Jo, S., Lee, J.B., Jin, Y., Jeong, T., Yoon, J.C., Park, B., 2020. Mortality
826 difference between early-identified sepsis and late-identified sepsis. Clin Exp
827 Emerg Med 7, 150–160.
828 Ju, Y., Kelly, H.G., Dagley, L.F., Reynaldi, A., Schlub, T.E., Spall, S.K., Bell, C.A., Cui, J.,
829 Mitchell, A.J., Lin, Z., Wheatley, A.K., Thurecht, K.J., Davenport, M.P., Webb, A.I.,
830 Caruso, F., Kent, S.J., 2020. Person-Specific Biomolecular Coronas Modulate
831 Nanoparticle Interactions with Immune Cells in Human Blood. ACS Nano 14,
832 15723–15737.
833 Khatoon, N., Zhang, Z., Zhou, C., Chu, M., 2022. Macrophage membrane coated
834 nanoparticles: a biomimetic approach for enhanced and targeted delivery. Biomater
835 Sci 10, 1193–1208.
836 Koide, H., Okishima, A., Hoshino, Y., Kamon, Y., Yoshimatsu, K., Saito, K., Yamauchi, I.,
837 Ariizumi, S., Zhou, Y., Xiao, T.-H., Goda, K., Oku, N., Asai, T., Shea, K.J., 2021a.
838 Synthetic hydrogel nanoparticles for sepsis therapy. Nat Commun 12, 5552.
839 Koide, H., Okishima, A., Hoshino, Y., Kamon, Y., Yoshimatsu, K., Saito, K., Yamauchi, I.,
840 Ariizumi, S., Zhou, Y., Xiao, T.-H., Goda, K., Oku, N., Asai, T., Shea, K.J., 2021b.
841 Synthetic hydrogel nanoparticles for sepsis therapy. Nat Commun 12, 5552.
842 Lasola, J.J.M., Kamdem, H., McDaniel, M.W., Pearson, R.M., 2020. Biomaterial-Driven
843 Immunomodulation: Cell Biology-Based Strategies to Mitigate Severe Inflammation
844 and Sepsis. Front Immunol 11.
845 Li, X., Bao, H., Wang, Z., Wang, M., Fan, B., Zhu, C., Chen, Z., 2018. Biogenesis and
846 function of multivesicular bodies in plant immunity. Front Plant Sci 9.

847 Lima, A.C., Cunha, C., Carvalho, A., Ferreira, H., Neves, N.M., 2018. Interleukin-6
848 Neutralization by Antibodies Immobilized at the Surface of Polymeric Nanoparticles
849 as a Therapeutic Strategy for Arthritic Diseases. ACS Appl Mater Interfaces 10,
850 13839–13850.
851 Liu, C., Zhao, X.-M., Wang, Q., Du, T.-T., Zhang, M.-X., Wang, H.-Z., Li, R.-P., Liang, K.,
852 Gao, Y., Zhou, S.-Y., Xue, T., Zhang, J.-G., Han, C.-L., Shi, L., Zhang, L.-W., Meng,
853 F.-G., 2023. Astrocyte-derived SerpinA3N promotes neuroinflammation and
854 epileptic seizures by activating the NF-κB signaling pathway in mice with temporal
855 lobe epilepsy. J Neuroinflammation 20, 161.
856 Liu, T., Zhang, L., Joo, D., Sun, S.-C., 2017. NF-κB signaling in inflammation. Signal
857 Transduct Target Ther 2, 17023.
858 Markanday, A., 2015a. Acute Phase Reactants in Infections: Evidence-Based Review
859 and a Guide for Clinicians. Open Forum Infect Dis 2, ofv098.
860 Markanday, A., 2015b. Acute Phase Reactants in Infections: Evidence-Based Review
861 and a Guide for Clinicians. Open Forum Infect Dis 2, ofv098.
862 Massart, I.S., Paulissen, G., Loumaye, A., Lause, P., Pötgens, S.A., Thibaut, M.M.,
863 Balan, E., Deldicque, L., Atfi, A., Louis, E., Gruson, D., Bindels, L.B., Meuwis, M.-
864 A., Thissen, J.-P., 2020. Marked Increased Production of Acute Phase Reactants by
865 Skeletal Muscle during Cancer Cachexia. Cancers (Basel) 12.
866 Matyash, V., Liebisch, G., Kurzchalia, T. V, Shevchenko, A., Schwudke, D., 2008. Lipid
867 extraction by methyl-tert-butyl ether for high-throughput lipidomics. J Lipid Res 49,
868 1137–1146.

869 Mera, S., Tatulescu, D., Cismaru, C., Bondor, C., Slavcovici, A., Zanc, V., Carstina, D.,
870 Oltean, M., 2011. Multiplex cytokine profiling in patients with sepsis. APMIS 119,
871 155–163.
872 Messina, J.M., Luo, M., Hossan, M.S., Gadelrab, H.A., Yang, X., John, A., Wilmore,
873 J.R., Luo, J., 2024. Unveiling cytokine charge disparity as a potential mechanism
874 for immune regulation. Cytokine Growth Factor Rev 77, 1–14.
875 Miller, A.H., Raison, C.L., 2016. The role of inflammation in depression: from
876 evolutionary imperative to modern treatment target. Nat Rev Immunol 16, 22–34.
877 Miller, S.D., Turley, D.M., Podojil, J.R., 2007. Antigen-specific tolerance strategies for
878 the prevention and treatment of autoimmune disease. Nat Rev Immunol 7, 665–
879 677.
880 Nyati, K.K., Masuda, K., Zaman, M.M.-U., Dubey, P.K., Millrine, D., Chalise, J.P., Higa,
881 M., Li, S., Standley, D.M., Saito, K., Hanieh, H., Kishimoto, T., 2017. TLR4-induced
882 NF-κB and MAPK signaling regulate the IL-6 mRNA stabilizing protein Arid5a.
883 Nucleic Acids Res 45, 2687–2703.
884 Parisi, L., Gini, E., Baci, D., Tremolati, M., Fanuli, M., Bassani, B., Farronato, G., Bruno,
885 A., Mortara, L., 2018. Macrophage Polarization in Chronic Inflammatory Diseases:
886 Killers or Builders? J Immunol Res 2018, 8917804.
887 Pearson, R.M., Juettner, V. V, Hong, S., 2014. Biomolecular corona on nanoparticles: a
888 survey of recent literature and its implications in targeted drug delivery. Front Chem
889 2.

890 Perut, F., Roncuzzi, L., Avnet, S., Massa, A., Zini, N., Sabbadini, S., Giampieri, F.,
891 Mezzetti, B., Baldini, N., 2021. Strawberry-Derived Exosome-Like Nanoparticles
892 Prevent Oxidative Stress in Human Mesenchymal Stromal Cells. Biomolecules 11.
893 Popa, C., Netea, M.G., van Riel, P.L.C.M., van der Meer, J.W.M., Stalenhoef, A.F.H.,
894 2007. The role of TNF-α in chronic inflammatory conditions, intermediary
895 metabolism, and cardiovascular risk. J Lipid Res 48, 751–762.
896 Robards, a.w., kidwai, p., 1969. vesicular involvement in differentiating plant vascular
897 cells. New Phytologist 68, 343–349.
898 Shao, H., Im, H., Castro, C.M., Breakefield, X., Weissleder, R., Lee, H., 2018. New
899 Technologies for Analysis of Extracellular Vesicles. Chem Rev 118, 1917–1950.
900 Shaw, J., Pearson, R.M., 2022. Nanoparticle personalized biomolecular corona:
901 implications of pre-existing conditions for immunomodulation and cancer. Biomater
902 Sci 10, 2540–2549.
903 Shen, H., Colangelo, C., Wu, T., Maffei, M., Goldstein, D.R., 2011. 235 Haptoglobin: A
904 Novel Innate Ligand that Induces Inflammation after Tissue Necrosis. J Heart Lung
905 Transplant 30, S84.
906 Shen, S., Han, F., Yuan, A., Wu, L., Cao, J., Qian, J., Qi, X., Yan, Y., Ge, Y., 2019.
907 Engineered nanoparticles disguised as macrophages for trapping
908 lipopolysaccharide and preventing endotoxemia. Biomaterials 189, 60–68.
909 Shi, C., Wang, X., Wang, L., Meng, Q., Guo, D., Chen, L., Dai, M., Wang, G., Cooney,
910 R., Luo, J., 2020a. A nanotrap improves survival in severe sepsis by attenuating
911 hyperinflammation. Nat Commun 11, 3384.

912 Shi, C., Wang, X., Wang, L., Meng, Q., Guo, D., Chen, L., Dai, M., Wang, G., Cooney,
913 R., Luo, J., 2020b. A nanotrap improves survival in severe sepsis by attenuating
914 hyperinflammation. Nat Commun 11, 3384.
915 Sung, J., Yang, C., Viennois, E., Zhang, M., Merlin, D., 2019. Isolation, Purification, and
916 Characterization of Ginger-derived Nanoparticles (GDNPs) from Ginger, Rhizome
917 of Zingiber officinale. Bio Protoc 9, e3390.
918 Tanaka, T., Narazaki, M., Kishimoto, T., 2014. IL-6 in Inflammation, Immunity, and
919 Disease. Cold Spring Harb Perspect Biol 6, a016295–a016295.
920 Tenci, B., Di Cesare Mannelli, L., Maresca, M., Micheli, L., Pieraccini, G., Mulinacci, N.,
921 Ghelardini, C., 2017. Effects of a water extract of Lepidium meyenii root in different
922 models of persistent pain in rats. Zeitschrift für Naturforschung C 72, 449–457.
923 Thamphiwatana, S., Angsantikul, P., Escajadillo, T., Zhang, Q., Olson, J., Luk, B.T.,
924 Zhang, S., Fang, R.H., Gao, W., Nizet, V., Zhang, L., 2017a. Macrophage-like
925 nanoparticles concurrently absorbing endotoxins and proinflammatory cytokines for
926 sepsis management. Proc Natl Acad Sci 114, 11488–11493.
927 Torres, A., Vivanco, S., Lavín, F., Pereda, C., Chernobrovkin, A., Gleisner, A., Alcota, M.,
928 Larrondo, M., López, M.N., Salazar-Onfray, F., Zubarev, R.A., González, F.E., 2022.
929 Haptoglobin Induces a Specific Proteomic Profile and a Mature-Associated
930 Phenotype on Primary Human Monocyte-Derived Dendritic Cells. Int J Mol Sci 23.
931 Truong, N., Black, S.K., Shaw, J., Scotland, B.L., Pearson, R.M., 2021. Microfluidic-
932 Generated Immunomodulatory Nanoparticles and Formulation-Dependent Effects
933 on Lipopolysaccharide-Induced Macrophage Inflammation. AAPS J 24, 6.

934 Truong, N., Cottingham, A.L., Dharmaraj, S., Shaw, J.R., Lasola, J.J.M., Goodis, C.C.,
935 Fletcher, S., Pearson, R.M., 2024. Multimodal nanoparticle-containing modified
936 suberoylanilide hydroxamic acid polymer conjugates to mitigate immune
937 dysfunction in severe inflammation. Bioeng Transl Med 9, e10611.
938 Unsinger, J., McGlynn, M., Kasten, K.R., Hoekzema, A.S., Watanabe, E., Muenzer, J.T.,
939 McDonough, J.S., Tschoep, J., Ferguson, T.A., McDunn, J.E., Morre, M., Hildeman,
940 D.A., Caldwell, C.C., Hotchkiss, R.S., 2010. IL-7 Promotes T Cell Viability,
941 Trafficking, and Functionality and Improves Survival in Sepsis. The J Immunology
942 184, 3768–3779.
943 Wang, Q., Zhuang, X., Mu, J., Deng, Z.-B., Jiang, H., Zhang, L., Xiang, X., Wang, B.,
944 Yan, J., Miller, D., Zhang, H.-G., 2013. Delivery of therapeutic agents by
945 nanoparticles made of grapefruit-derived lipids. Nat Commun 4, 1867.
946 Wang, S., Zhu, F., 2019. Chemical composition and health effects of maca (Lepidium
947 meyenii). Food Chem 288, 422–443.
948 Wu, H.-P., Chen, C.-K., Chung, K., Tseng, J.-C., Hua, C.-C., Liu, Y.-C., Chuang, D.-Y.,
949 Yang, C.-H., 2009. Serial cytokine levels in patients with severe sepsis. Inflamm
950 Res 58, 385–393.
951 Yang, C., Long, D., Sung, J., Alghoul, Z., Merlin, D., 2021. Orally Administered Natural
952 Lipid Nanoparticle-Loaded 6-Shogaol Shapes the Anti-Inflammatory Microbiota and
953 Metabolome. Pharmaceutics 13.
954 Yang, J., Cho, H., Gil, M., Kim, K.E., 2023. Anti-Inflammation and Anti-Melanogenic
955 Effects of Maca Root Extracts Fermented Using Lactobacillus Strains. Antioxidants
956 12.

957 Ye, R.D., Sun, L., 2015. Emerging functions of serum amyloid A in inflammation. J
958 Leukoc Biol 98, 923–929.
959 Zhang, Q., Hu, Chengyi, Feng, J., Long, H., Wang, Y., Wang, P., Hu, Chenglu, Yue, Y.,
960 Zhang, C., Liu, Z., Zhou, X., 2024. Anti-inflammatory mechanisms of neutrophil
961 membrane-coated nanoparticles without drug loading. J Control Release 369, 12–
962 24.
963 Zhang, Y., Ning, B., 2021. Signaling pathways and intervention therapies in sepsis.
964 Signal Transduct Target Ther 6, 407.
965 Zhu, H., Wang, R., Hua, H., Qian, H., Du, P., 2022. Deciphering the potential role of
966 Maca compounds prescription influencing gut microbiota in the management of
967 exercise-induced fatigue by integrative genomic analysis. Front Nutr 9.
968
969

970 **List of Figure Captions**
971
972 **Figure 1**. Isolation and characterization of MDNP. (A) Schematic representation of the
973 isolation process for maca-derived lipid nanoparticles (MDNP). (B) Before and after
974 images of MDNP isolation. MDNP were isolated and purified from maca extract by
975 sucrose density gradient purification. (C) MDNP recovery from pure maca powder. (D) A
976 representative TEM image of MDNP. (E) Room temperature measurement of size (174.5
977 nm) and zeta potential (-9.6 mV) of freshly isolated MDNP. (F) Storage stability test of
978 MDNP under various storage conditions up to day 6. (G) Heat flow curve of MDNP
979 measured by differential scanning calorimetry showing the summit of melting peak at 74.3
980 ºC. (H) Lipid extraction and component analysis by liquid chromatography coupled to high
981 resolution LC-MS/MS revealed eight different lipids (TG, Cer, HexCer, DGDG, LPC, PC,
982 PI and FFA). Bar graph shows abundance of lipids. (I) Pie graph shows the whole ratio of
983 each component and the vertical slice magnifies the smaller portion of composition
984 excluding TG. N=3/group.
985
986 **Figure 2.** *In vitro* cytotoxicity, cellular internalization, immunomodulation and therapeutic
987 effects against LPS-induced inflammation. (A) PI/Annexin V assay by flow cytometry
988 displayed that treatment with higher concentration (1 mg/mL) of MDNP did not induce any
989 significant toxicity in BMDM. Quantitative analysis of live, apoptotic, and dead cells after
990 MDNP treatment is accompanied. (B) Cy5.5 labeled MDNP were gradually internalized
991 by BMDM after 4 and 8 hrs. Cells were stained with DAPI and FITC-PI to visualize the
992 nucleus and F-actin, respectively. (C-F) Immunomodulatory activity of MDNP in LPS
993 inflamed BMDM showed reduction in M1 (CD80, CD86, MHCII) and M2 (CD206) markers

994 (G) A timeline for prophylactic treatment. Prophylactic approach did not make significant
995 change in levels of (H) IL-6 and (I) TNF-α. (J) A timeline for therapeutic treatment.
996 Therapeutic treatment displayed significant reduction of (K) IL-6 and (L) TNF-α. Data are
997 expressed as mean ± SD (n=5). Data are expressed as mean ± SD (n=3). *P<0.05,
998 **p<0.05 versus LPS control group.
999
1000 **Figure 3.** *In vitro* sequestration of pro-inflammatory cytokines from LPS-induced bone
1001 marrow derived macrophages. (A) Time course reduction of LPS-stimulated pro-
1002 inflammatory cytokine by treatment of MDNP. 8 hr time point exhibited the most significant
1003 reduction for both (B) IL-6 and (C) TNF-α. (D) Recombinant IL-6 was sequestered through
1004 incubation with MDNP ex vivo without cellular interaction. (E) 100 μg/mL MDNP was the
1005 most effective concentration to remove IL-6 protein. (F) Expression of NF-κB in in RAW-
1006 Blue 264.7 cell is suppressed by the treatment of MDNP. (G) NF-κB activity level is
1007 downregulated after treatment of MDNP. PLGA was used as a control to show different
1008 effect on NF-κB. All data are expressed as means ± SD (n=5). **p<0.05, ***p<0.005, and
1009 ****p<0.0005 versus LPS or NT control group.
1010
1011 **Figure 4**. Route of administration biodistribution and anti-inflammatory effects of MDNP
1012 (A) Timeline of MDNP treatments following LPS challenge. The schematic illustrates the
1013 IP and IV injection performed on randomly selected C57BL/6J mice groups (LPS only,
1014 LPS+IP injection, and LPS+IV injection, n=3 per group). (B) Biodistribution of
1015 fluorescently labeled MDNP in mouse organs (liver, kidney, spleen, lung, and heart). (C)
1016 Fluorescence intensity measurement of MDNP biodistribution. (D) Heatmap of pro-

1017 inflammatory cytokine expression including: (E) IL-6, (F) TNF-α, (G) MCP-1, (H) IL-10, (I)
1018 IL-1β, (J) IFN-β, (K) GROα from mice plasma samples. Data are expressed as mean ±
1019 SD (n=3). *P<0.05, **p<0.05, ***p<0.005, and ****p<0.0005 versus PBS control group.
1020

1021 **Figure 5.** Representative images of organ recovery and survival effect by treatment of
1022 MDNP during LPS-induced sepsis. (A) H&E staining of liver, kidney, spleen, lung, and
1023 heart. The LPS treated group images shows presence of neutrophil infiltration (yellow
1024 arrow) in liver, tubular necrosis (white arrow) in the tubules in kidney, focal necrosis and
1025 dysregulation in white pulp of spleen, appearance of extensive clots (red arrow) in the
1026 alveoli in lungs, while no noticeable damage in heart. On the contrary, mice organs
1027 administered with IP and IV displayed notably reduced level of organ damage of organ
1028 damage. (B-F) Quantification of H&E staining. Levels of injury scores were calculated.
1029 Data are expressed as mean ± SD (n=3). *P<0.05, **p<0.05 versus LPS control group.
1030 (G) A schematic of survival study of LPS-treated and LPS+MDNP-treated C57BL/6J mice
1031 (n=10/group). (H) The survival analysis graph displays a significant difference between
1032 LPS only and the MDNP treatment group. Kaplan-Meier curves and a log-rank test was
1033 performed to compare the survival rates. ***p<0.0005.
1034

1035 **Figure 6**. Mapping and identification of protein corona adsorbed onto the surface of
1036 MDNP. (A) A schematic showing the process of evaluating the MDNP protein corona. (B)
1037 Venn diagram illustrating a total of 296 proteins detected including unique (1 in healthy
1038 and 26 in LPS) and 270 shared proteins in the coronas. (C) Heatmap shows abundance
1039 of 49 upregulated and 100 downregulated proteins in MDNP-LPS group compared to

1040 MDNP-H healthy group. (D) Volcano plot of significantly upregulated and downregulated
1041 corona proteins. Hp, Serpina3n and Saa1 (red dots) are categorized as pro-inflammatory
1042 and acute phase response signaling proteins. (E) Top 10 canonical pathways associated
1043 with the significantly upregulated protein corona were identified, with acute phase
1044 response signaling being the most prominent pathway. (F) A network representation of
1045 acute phase response signaling proteins and major upstream regulators. (G) *Ex vivo*
1046 sequestration of pro-inflammatory cytokines by incubating LPS plasma with MDNP. Both
1047 IL-6 and TNF-α was significantly reduced by 8 hr treatment. (H) A graphical summary
1048 illustrating how the cytokine and acute phase protein corona-coated MDNP sequesters
1049 and neutralizes inflammatory proteins, thereby reducing overall inflammation.
1050
1051 **Figure 7.** Survival effects of MDNP treatment on severe CLP model. (A) Schematic
1052 timeline of survival study of cecal ligation and puncture (CLP) C57BL/6J murine model
1053 with MDNP treatment (n=5/group) based on the complement cascade pathway from
1054 proteomics. Mice underwent CLP surgery to induce severe polymicrobial inflammation
1055 and three separate doses of MDNP were administered intraperitoneally (0.5, 2, 24 hr
1056 timepoint, 2 mg/injection) to analyze survival. (B) *Ex vivo* sequestration test of CLP
1057 plasma and MDNP showed that both IL-6 and TNF-α was significantly reduced. Kaplan-
1058 Meier curves and a log-rank test was performed to compare the survival rates. (C) The
1059 survival test displayed a significant improvement (40%) by the treatment of MDNP **p<
1060 0.005. Data are expressed as mean ± SD (n=5). ****p<0.0005 versus PBS control group.
1061
1062
1063
1064

1065 # Tables

1066

1067 **Table 1.** A list of unique proteins that are part of the MDNP protein corona formed from LPS and healthy plasma.
1068 A total 26 proteins are derived from the LPS plasma protein corona, while only one unique protein is found in
1069 healthy plasma corona. Acute phase proteins are highlighted with circles to underscore the potential presence of pro-inflammatory proteins associated with MDNP.

Protein Corona	Accession	Description	Gene Symbol	Function	Acute Phase Protein
LPS Plasma	Q8BMT4	Transforming growth factor beta activator LRRC33	Nrros	Key regulator of TGFB1 required for microglia function in nervous system	
	Q9Z1T2	Thrombospondin-4	Thbs4	Adhesive glycoprotein that mediates cell-to-cell interaction	
	P39876	Metalloproteinase inhibitor 3	Timp3	Regulates hematopoietic stem cell proliferation, differentiation, and trafficking	
	P02089	Hemoglobin subunit beta-2	Hbb-b2	Oxygen, CO2 transport and pH regulation	
	P62806	Histone H4	H4	Central role in transciption regulation, DNA repair and replication	
	P10810	Monocyte differentiation antigen CD14	Cd14	Co-receptor for TLR4 and recognize LPS and PAMPs	O
	P11672	Neutrophil gelatinase-associated lipocalin	Lcn2	Regulates neutrophil recruitment and modulatess pro-inflammatory cytokines	O
	P14152	Malate dehydrogenase, cytoplasmic	Mdh1	Involved in Krebs cycle and plays critical role in cellular energy production	
	P12246	Serum amyloid P-component	Apcs	Acute-phase reactant that bind to complement protetins and damaged cell	O
	P04117	Fatty acid-binding protein, adipocyte	Fabp4	Regulates choesterol ester accumulation and inflammatory responses	O
	P32848	Parvalbumin alpha	Pvalb	Calcium-binding protein involved in regulation of Ca2+ levels in neurons to muscle	
	P70296	Phosphatidylethanolamine-binding protein 1	Pebp1	Regulate the trafficking and distribution of phosphotidylethanolamine within cells	
	Q99PT1	Rho GDP-dissociation inhibitor 1	Arhgdia	Inhibits GDP/GTP exchange activity of Rho GTPases	
	O08692	Neutrophilic granule protein	Ngp	Enzymatic activity that break down bacterial wall that damaged bacterial DNA	
	Q64339	Ubiquitin-like protein ISG15	Isg15	Antiviral defense by degradating viral proteins and modulate immune response	
	P09411	Phosphoglycerate kinase 1	Pgk1	Catalyze the reversible transfer of a phosphate group between 1,3-BPG and ADP	
	P48774	Glutathione S-transferase Mu 5	Gstm5	Catalyze the conjugation of GSH to electrophilic compound such as toxin and ROS	
	P70290	55 kDa erythrocyte membrane protein	Mpp1	Facilitate the exchange of Cl- and HCO2- across the erythrocyte membrane	
	P07901	Heat shock protein HSP 90-alpha	Hsp90aa1	Involved in protein folding, stability and trafficking	O
	P54116	Stomatin	Stom	Maintain mechanical stability of erythrocyte membrane	
	O89103	Complement component C1q receptor	Cd93	Initiate the classical pathway of complement activation	
	P28666	Murinoglobulin-2	Mug2	Involved in cell adhesion, cell signalig regulation and contribute to barrier function	
	P49222	Protein 4.2	Epb42	Maintain stability and integrity of erythrocyte membrane	
	Q8BFZ3	Beta-actin-like protein 2	Actbl2	Involved in assembly and regulation of actn cytoskeleton	
	Q8VDD5	Myosin-9	Myh9	Transport vesicles and organelles within the cell	
	P63242	Eukaryotic translation initiation factor 5A-1	Eif5a	Facilitate the intiation of protein translation on ribosomes	
Healthy Plasma	Q14B46	Rhotekin-2	Rtkn2	Key regulator of actin cytoskeleton, cell signaling and cell adhesion	